

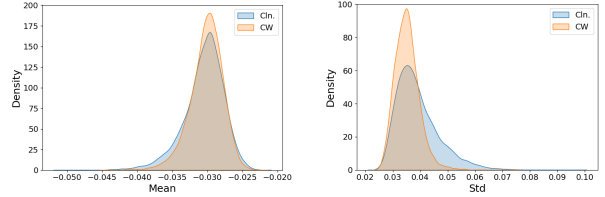
Feature Statistics with Uncertainty Help Adversarial Robustness

Ran Wang¹ Xinlei Zhou¹ Rihao Li¹ Meng Hu¹ Wenhui Wu² Yuheng Jia³

Abstract

Despite the remarkable success of deep neural networks (DNNs), the security threat of adversarial attacks poses a significant challenge to the reliability of DNNs. By introducing randomness into different parts of DNNs, stochastic methods can enable the model to learn some uncertainty, thereby improving model robustness efficiently. In this paper, we theoretically discover a universal phenomenon that adversarial attacks will shift the distributions of feature statistics. Motivated by this theoretical finding, we propose a robustness enhancement module called *Feature Statistics with Uncertainty* (FSU). It resamples channel-wise feature means and standard deviations of examples from multivariate Gaussian distributions, which helps to reconstruct the attacked examples and calibrate the shifted distributions. The calibration recovers some domain characteristics of the data for classification, thereby mitigating the influence of perturbations and weakening the ability of attacks to deceive models. The proposed FSU module has universal applicability in training, attacking, predicting and fine-tuning, demonstrating impressive robustness enhancement ability at trivial additional time cost. For example, against powerful optimization-based CW attacks, by incorporating FSU into attacking and predicting phases, it endows many collapsed state-of-the-art models with 50%~80% robust accuracy on CIFAR10, CIFAR100 and SVHN.

*Equal contribution ¹School of Mathematical Sciences, Shenzhen University, Shenzhen, China ²College of Electronic and Information Engineering, Shenzhen University, Shenzhen, China ³School of Computer Science and Engineering, Southeast University, Nanjing, China. Correspondence to: Ran Wang <wangran@szu.edu.cn>, Xinlei Zhou <zhouxnli@szu.edu.cn>, Rihao Li <2450191005@mails.szu.edu.cn>, Meng Hu <huhmeng@szu.edu.cn>, Wenhui Wu <wuwenhui@szu.edu.cn>, Yuheng Jia <yhjia@seu.edu.cn>.



(a) Shift of Feature Mean

(b) Shift of Feature Std

Figure 1. Distribution shifts of feature statistics (mean and Std) of attacked examples in CIFAR10 (average of 512 channels in latent space). “Cln.” and “CW” represent clean examples and examples disturbed by CW attack, respectively.

1. Introduction

Deep neural networks (DNNs) are vulnerable to adversarial attacks (Szegedy et al., 2014), which fool the deployed models into making false predictions by adding subtle perturbations to clean examples. Adversarial training (Madry et al., 2018; Shafahi et al., 2019) and its variants (e.g., TRADES (Zhang et al., 2019), MART (Wang et al., 2020), AT-AWP (Wu et al., 2020), MLCAT_{WP} (Yu et al., 2022), AT+RiFT (Zhu et al., 2023), etc.) are the most mainstream defense methods to endow a DNN model with robustness. However, the training cost is usually several times or even dozens of times more expensive than natural training. Meanwhile, the ability to generalize on clean examples might be sacrificed.

Recent studies have revealed that stochastic methods can learn some uncertainty by introducing randomness into the networks, thereby improving model robustness very efficiently. A group of works focuses on *feature uncertainty*. For example, smoothed classifiers are obtained for certified robustness by applying random smoothing technique (Cohen et al., 2019). The input data is augmented by random transformation (Xie et al., 2018) or Gaussian noise injection (Li et al., 2019) to resist perturbations. Random noises are injected into the hidden layer features with a hyperparameter diagonal variance matrix (Liu et al., 2018a) or a fully parameterized variance matrix (Eustratiadis et al., 2021; Yang et al., 2023a;b). Moreover, the deep variational information bottleneck method (Alemi et al., 2017) is adopted in (Wang et al., 2024) to learn uncertain feature representations, together with a label embedding module, etc. Another group of works focuses on *weight uncertainty*. For example,

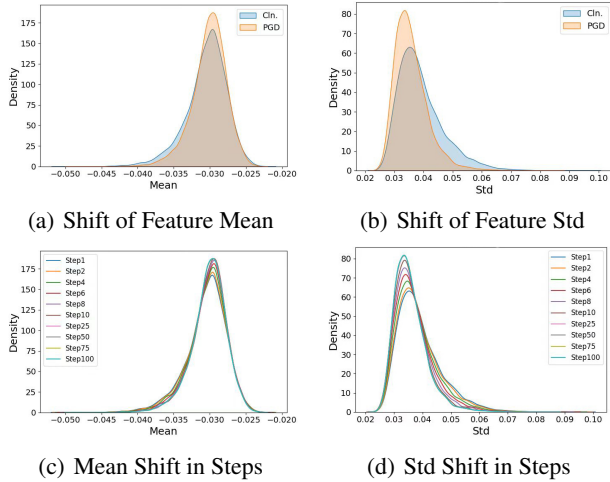


Figure 2. Distribution shifts of feature statistics (mean and Std) of attacked examples in CIFAR10 (average of 512 channels in latent space). “Cln.” and “PGD” represent clean examples and examples disturbed by PGD-100 attack, respectively.

Adv-bnn (Liu et al., 2018b) treats the network parameters as random variables rather than deterministic numbers, and learns the parameter distributions as in Bayesian neural networks (Carbone et al., 2020). Parametric noise injection (PNI) method (He et al., 2019) designs a learnable noise injection strategy for the weights of each hidden layer. Learn2Perturb (L2P) method (Jeddi et al., 2020) adopts alternating back-propagation to consecutively train the noise parameters, etc.

The above stochastic methods, whether focusing on feature uncertainty or weight uncertainty, introduce randomness to individual examples or nodes. Many of them have difficulties capturing class-level or domain-level characteristics, subsequently fail against powerful attacks, e.g., (Carlini & Wagner, 2017; Croce & Hein, 2020).

It is argued in (Li et al., 2022) that *feature statistics (such as mean and variance)* carry domain characteristics of training data, which help improve out-of-distribution generalization. Under the assumption that feature mean and standard deviation follow Gaussian distributions, random noises are sampled to model their uncertainty, in order to alleviate the perturbations against potential domain shifts. Inspired by this work, we are encouraged to promote model robustness by using *Feature Statistics with Uncertainty (FSU)*. Ideally, the disturbed examples can be reconstructed by resampling their feature means and standard deviations from Gaussian distributions. Batch-level statistical information is used to estimate the distribution parameters, such that some domain characteristics for classification can be recovered. To summarize, our proposed method has the following merits:

- Both theoretically and empirically, we discover an important phenomenon that adversarial attacks will

change the mean or variance of feature statistics, thereby causing some potential distribution shifts.

- We propose an FSU module, which calibrates the distribution shifts and reconstructs perturbed examples in latent space by resampling their feature means and standard deviations based on batch-level statistical information. Since FSU has no parameters to learn, it can be employed in both training and testing (including attacking and predicting) phases.
- The FSU module does not rely on adversarial information, thus is applicable in both natural training and adversarial training. By introducing some directional information at the feature statistic-level, it can also be used for fine-tuning any well-established models.
- Extensive experiments under various settings demonstrate the universal applicability of FSU for robustness enhancement, e.g., under powerful optimization-based Carlini & Wagner’s (CW) attack, FSU endows many collapsed state-of-the-art models with **50%~80%** robust accuracy on benchmark datasets.

2. Theoretical and Empirical Analysis

Given a dataset $\mathbb{D} = \{(\mathbf{x}_i, y_i)\}_{i=1}^N$ and a trained network model F_θ , the essence of generating adversarial example for any $(\mathbf{x}, y) \in \mathbb{D}$, i.e., $\mathbf{x}' = \mathbf{x} + \delta$, is to solve the following optimization problem:

$$\max_{\delta} \mathcal{L}(F_\theta(\mathbf{x} + \delta), y), \text{ s.t. } \|\delta\| < \epsilon, \quad (1)$$

where δ is the perturbation generated for \mathbf{x} , y is the ground truth label of \mathbf{x} , θ is the network parameter, $\mathcal{L}(\cdot)$ is the loss function, ϵ is the upper bound limit of δ , and $\|\cdot\|$ is usually taken as l_0 , l_2 or l_∞ norm.

As for defending against adversarial attacks, the essence is to improve the robustness of F by optimizing θ or by reconstructing $\mathbf{x} + \delta$ such that $F_\theta(\mathbf{x} + \delta) = F_\theta(\mathbf{x}) = y$.

Suppose the set of clean examples $\mathbf{x}_1, \mathbf{x}_2, \dots, \mathbf{x}_N$ are attacked into adversarial examples $\mathbf{x}'_1, \mathbf{x}'_2, \dots, \mathbf{x}'_N$ through F_θ . Let μ_i and μ'_i be the feature means of \mathbf{x}_i and \mathbf{x}'_i ; let σ_i and σ'_i be the feature standard deviations of \mathbf{x}_i and \mathbf{x}'_i . With a high probability, the following propositions hold.

Proposition 2.1. *The variance of feature means becomes smaller after being attacked, i.e., $\text{var}(\mu') \leq \text{var}(\mu)$.*

Proposition 2.2. *The mean of feature variances becomes smaller after being attacked, i.e., $\mathbb{E}(\sigma'^2) \leq \mathbb{E}(\sigma^2)$.*

Proposition 2.3. *The variance of feature variances becomes smaller after being attacked, i.e., $\text{var}(\sigma'^2) \leq \text{var}(\sigma^2)$.*

The proofs of **Propositions 2.1, 2.2** and **2.3** are in Appendices A, B and C, respectively. Obviously, if these propositions hold, we can recover some domain characteristics of

data by enlarging the mean or variance of feature statistics of attacked examples, so as to alleviate perturbations and enhance robustness.

As empirical verifications, Figs. 1~2 demonstrate the distributions of latent feature mean and standard deviation (Std) of both clean examples and attacked examples in CIFAR10. The model is trained by MLCAT_{WP} (Yu et al., 2022) with PreAct ResNet-18 architecture, and the distributions are obtained by kernel density estimation. Fig. 1 and Fig. 2 correspond to l_2 -norm CW attack and l_∞ -norm 100-step projected gradient descent (PGD-100) attack with step size $\epsilon/10$, respectively, where the attack strength is $\epsilon = 8/255$. Obviously, both of these two attacks cause distribution shifts of feature statistics. Especially, the variances of both feature mean and standard deviation become smaller, indicating that the difference among examples becomes weaker, causing difficulties for the model to distinguish them.

3. Proposed Method

3.1. Basic Idea

Given an image classification task, where the images are fed into a multi-channel network batch-by-batch. Considering a batch of examples, we investigate the feature maps in a multi-channel hidden layer, and denote $\mathbf{z}_{b,c}$ as the feature map of the b -th example in the c -th channel, i.e.,

$$\mathbf{z}_{b,c} = \begin{bmatrix} z_{b,c}^{1,1} & \cdots & z_{b,c}^{1,W} \\ \vdots & \ddots & \vdots \\ z_{b,c}^{H,1} & \cdots & z_{b,c}^{H,W} \end{bmatrix}_{H \times W}, \quad (2)$$

where $b = 1, \dots, B$ (B is the batch size), $c = 1, \dots, C$ (C is the number of channels), H and W are the height and width of the feature map, respectively. Easily, we can compute

$$\begin{cases} \mu_{b,c} = \mathbb{E}(z_{b,c}^{i,j}) = \frac{1}{HW} \sum_{i=1}^H \sum_{j=1}^W z_{b,c}^{i,j} \\ \sigma_{b,c} = \sqrt{\frac{1}{HW} \sum_{i=1}^H \sum_{j=1}^W (z_{b,c}^{i,j} - \mathbb{E}[z_{b,c}^{i,j}])^2} \end{cases}. \quad (3)$$

Obviously, $\mu_{b,c}$ and $\sigma_{b,c}$ are the two most important feature statistics of $\mathbf{z}_{b,c}$, which respectively reflect the average and dispersion of features in $\mathbf{z}_{b,c}$. When the batch size B is large enough, it is reasonable to assume that $\mu_{b,c}$ and $\sigma_{b,c}$ approximately follow Gaussian distributions.

Given a clean feature map $\mathbf{z}_{b,c}$, its $\mu_{b,c}$ and $\sigma_{b,c}$ can be easily computed according to Eq. (3). When $\mathbf{z}_{b,c}$ is disturbed by the attacker, $\mu_{b,c}$ and $\sigma_{b,c}$ will change correspondingly. All the attacked feature maps together cause possible distribution shifts as in Figs. 1~2. Since the clean distributions keep some useful domain characteristics for classification, if all $\mu_{b,c}$ and $\sigma_{b,c}$ can be resampled, it is possible to calibrate the shifted distributions and reconstruct the attacked feature maps, thereby enhancing robustness.

Our basic idea is to insert an FSU module after a certain hidden layer of the backbone architecture, which resamples the channel-wise feature means and standard deviations of each example according to statistical information in the batch. After the new feature means and standard deviations are obtained, the feature maps are reconstructed and inputted into the remaining layers of the network.

3.2. The FSU Module

A schematic view of the FSU module is provided in Fig. 3. In specific, given a (possibly disturbed) feature map $\mathbf{z}_{b,c}$, its mean $\mu_{b,c}$ and standard deviation $\sigma_{b,c}$ are supposed to follow Gaussian distributions, i.e.,

$$\begin{cases} \mu_{b,c} \sim \mathcal{N}(\Phi_{\mu_c}, \Sigma_{\mu_c}^2) \\ \sigma_{b,c} \sim \mathcal{N}(\Phi_{\sigma_c}, \Sigma_{\sigma_c}^2) \end{cases}, \quad c = 1, \dots, C. \quad (4)$$

The channel-wise means of $\mu_{b,c}$ and $\sigma_{b,c}$ are estimated as

$$\begin{cases} \Phi_{\mu_c} = \mathbb{E}(\mu_{i,c}) = \frac{1}{B} \sum_{i=1}^B \mu_{i,c} \\ \Phi_{\sigma_c} = \mathbb{E}(\sigma_{i,c}) = \frac{1}{B} \sum_{i=1}^B \sigma_{i,c} \end{cases}, \quad c = 1, \dots, C, \quad (5)$$

and the channel-wise standard deviations of $\mu_{b,c}$ and $\sigma_{b,c}$ are estimated as

$$\begin{cases} \Sigma_{\mu_c} = \sqrt{\frac{1}{B} \sum_{i=1}^B (\mu_{i,c} - \Phi_{\mu_c})^2} \\ \Sigma_{\sigma_c} = \sqrt{\frac{1}{B} \sum_{i=1}^B (\sigma_{i,c} - \Phi_{\sigma_c})^2} \end{cases}, \quad c = 1, \dots, C. \quad (6)$$

Following the theoretical findings in Section 2, to recover some domain characteristics (i.e., distinctions of the examples) for classification, we need to enlarge the variances of $\mu_{b,c}$ and $\sigma_{b,c}$. Let $\hat{\mu}_{b,c}$ and $\hat{\sigma}_{b,c}$ be the new $\mu_{b,c}$ and $\sigma_{b,c}$, to achieve this goal, they can be obtained by biased resampling from $\mathcal{N}(\mu_{b,c}, \Sigma_{\mu_c}^2)$ and $\mathcal{N}(\sigma_{b,c}, \Sigma_{\sigma_c}^2)$, respectively.

Since the sampling process cannot be incorporated into gradient-based back-prorogation training, we apply the reparameterization trick to achieve this goal. Let $\epsilon_{b,c}^\mu$ and $\epsilon_{b,c}^\sigma$ respectively be the *uncertain correction terms* for $\mu_{b,c}$ and $\sigma_{b,c}$, which are randomly and independently drawn from standard Gaussian distribution $\mathcal{N}(0, 1)$, i.e.,

$$\begin{cases} \epsilon_{b,c}^{\mu} \sim \mathcal{N}(0, 1) \\ \epsilon_{b,c}^{\sigma} \sim \mathcal{N}(0, 1) \end{cases}, \quad b = 1, \dots, B, \quad c = 1, \dots, C. \quad (7)$$

Then, the feature mean and standard deviation of $\mathbf{z}_{b,c}$ are reconstructed as

$$\begin{cases} \hat{\mu}_{b,c} = \mu_{b,c} + \alpha \cdot \epsilon_{b,c}^\mu \cdot \Sigma_{\mu_c} \\ \hat{\sigma}_{b,c} = \sigma_{b,c} + \beta \cdot \epsilon_{b,c}^\sigma \cdot \Sigma_{\sigma_c} \end{cases}, \quad (8)$$

where α and β are the noise intensities for feature mean and standard deviation, respectively. Having the resampled $\hat{\mu}_{b,c}$ and $\hat{\sigma}_{b,c}$, $\mathbf{z}_{b,c}$ is finally reconstructed as

$$\hat{\mathbf{z}}_{b,c} = \hat{\sigma}_{b,c} \times \frac{\mathbf{z}_{b,c} - \mu_{b,c}}{\sigma_{b,c}} + \hat{\mu}_{b,c}, \quad (9)$$

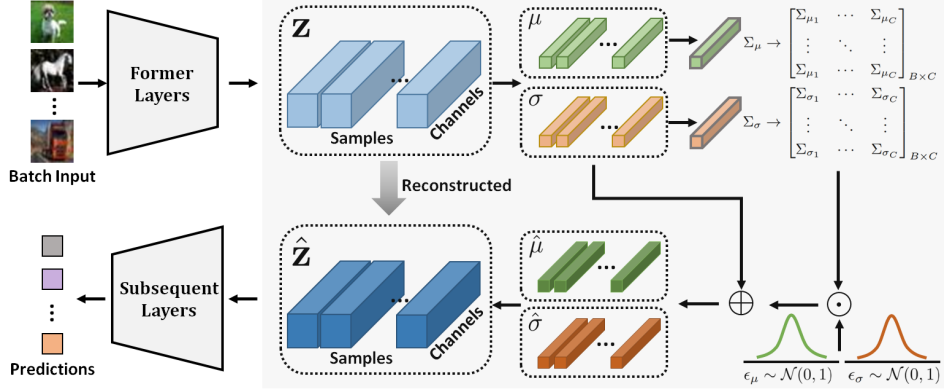


Figure 3. A schematic view of the proposed FSU module.

where the operations $-$, \times and $+$ indicate element-wise subtraction, multiplication, and addition, respectively, $b = 1, \dots, B$ and $c = 1, \dots, C$.

Note that the reconstruction depends only on the statistical information of the current batch, thus the FSU module can be independently employed in **training**, **attacking**, and **predicting** stages. In training, it encourages the network to learn some uncertainty via Gaussian noise; in attacking and predicting, it reconstructs features in each epoch to recover some domain characteristics for classification.

3.3. Intuitive Explanations

Theorem 3.1. Let $\hat{\mu}_{b,c}$ and $\hat{\sigma}_{b,c}$ be the reconstructed $\mu_{b,c}$ and $\sigma_{b,c}$ based on Eq. (8), then there are $\text{var}[\hat{\mu}_{b,c}] \geq \text{var}[\mu_{b,c}]$ and $\text{var}[\hat{\sigma}_{b,c}] \geq \text{var}[\sigma_{b,c}]$.

The proof of **Theorem 3.1** is in Appendix D.

Perspective 1 As presented in **Theorem 3.1**, the reconstruction can enlarge the variances of both the channel-wise mean and standard deviation of feature maps, thereby restoring some distinctions among examples and recovering some discriminative domain characteristics for classification.

Perspective 2 We derive an approximate distribution of the reconstructed features in Eq. (9). Unfortunately, when $\mu_{b,c}$, $\sigma_{b,c}$, $\hat{\mu}_{b,c}$, $\hat{\sigma}_{b,c}$ are all random variables, the inference on this distribution will be too complex, since it includes the division of two Gaussian distributions, as well as the multiplication of a Gaussian distribution and a ratio distribution. Given a specific example, $\mu_{b,c}$ and $\sigma_{b,c}$ can be treated as fixed values, and according to the proof of **Theorem 3.1** in Appendix D, we approximately let $\hat{\mu}_{b,c} \sim \mathcal{N}(\mu_{b,c}, (1 + \alpha^2)\Sigma_{\mu_c}^2)$ and $\hat{\sigma}_{b,c} \sim \mathcal{N}(\sigma_{b,c}, (1 + \beta^2)\Sigma_{\sigma_c}^2)$. Thus, according to Eq. (9), each feature $\hat{z}_{b,c}$ in feature map $\hat{\mathbf{z}}_{b,c}$ also follows Gaussian distribution, whose expectation is estimated as

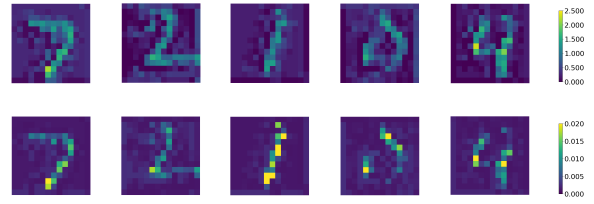


Figure 4. Feature maps (first line) and variance graphs calculated by Eq. (11) (second line) of FGSM-attacked examples in MNIST.

$$\begin{aligned} \mathbb{E}[\hat{z}_{b,c}] &= \mathbb{E}[\hat{\sigma}_{b,c}] \times \frac{z_{b,c} - \mu_{b,c}}{\sigma_{b,c}} + \mathbb{E}[\hat{\mu}_{b,c}] \\ &= \sigma_{b,c} \times \frac{z_{b,c} - \mu_{b,c}}{\sigma_{b,c}} + \mu_{b,c} \\ &= z_{b,c} \end{aligned}, \quad (10)$$

and variance is estimated as

$$\begin{aligned} \text{var}[\hat{z}_{b,c}] &= \text{var}[\hat{\sigma}_{b,c}] \left(\frac{z_{b,c} - \mu_{b,c}}{\sigma_{b,c}} \right)^2 + \text{var}[\hat{\mu}_{b,c}] \\ &= (1 + \alpha^2)\Sigma_{\sigma_c}^2 \left(\frac{z_{b,c} - \mu_{b,c}}{\sigma_{b,c}} \right)^2 + (1 + \beta^2)\Sigma_{\mu_c}^2 \end{aligned}. \quad (11)$$

Finally, we approximately have

$$\hat{z}_{b,c} \sim \mathcal{N} \left(z_{b,c}, (1 + \alpha^2)\Sigma_{\sigma_c}^2 \left(\frac{z_{b,c} - \mu_{b,c}}{\sigma_{b,c}} \right)^2 + (1 + \beta^2)\Sigma_{\mu_c}^2 \right). \quad (12)$$

Based on this approximate inference, $\hat{\mathbf{z}}_{b,c}$ is essentially a resampled feature map from a multivariate Gaussian distribution with mean $\mathbf{z}_{b,c}$ and variance determined by normalized $\mathbf{z}_{b,c}$ and the batch-level statistics $(\Sigma_{\mu_c}^2, \Sigma_{\sigma_c}^2)$. In pixel-level, if the feature value deviates more from the mean, the variance will be larger, and the amplitude of resampling will be greater. As empirical verifications, we establish an LeNet-5 model on dataset MNIST by natural training. Fig. 4 shows several fast gradient sign method (FGSM)-attacked feature maps, i.e., $\mathbb{E}[\hat{\mathbf{z}}_{b,c}]$, as well as the variance graphs calculated by Eq. (11), i.e., $\text{var}[\hat{\mathbf{z}}_{b,c}]$. Obviously, points with large variances correspond to significant features with important semantic information. Adversarial attacks make such significant feature points be less discriminative from the background, thus misleading the established model to

Algorithm 1 Model Fine-tuning with FSU

Input: Model F_θ , training set \mathbb{D} , learning rate η , attacking method, noise intensity factors $\alpha \geq 0$ and $\beta \geq 0$.
Output: Updated model F_θ .

```

for  $t = 1 : \text{num\_epoch}$  do
  for  $e = 1 : \text{num\_batch}$  do
    for each clean example  $\mathbf{x}$  in the batch do
      Apply attacking method to  $\mathbf{x}$  and get perturbed  $\mathbf{x}'$ ;
    end for
    Forward propagate the batch of  $\mathbf{x}$  and  $\mathbf{x}'$ :
    if reconstruction layer then
      Extract hidden feature maps of  $\mathbf{x}$  and  $\mathbf{x}'$ , i.e.  $\mathbf{z}$  and  $\mathbf{z}'$ ;
      Calculate channel-wise  $\mu$  and  $\sigma$  for each  $\mathbf{z}$ ;
      Calculate channel-wise  $\mu'$  and  $\sigma'$  for each  $\mathbf{z}'$ ;
      Calculate  $(\Sigma_{\mu'}, \Sigma_{\sigma'})$  for the batch of  $\mathbf{z}'$  via Eq. (6);
      if channel-wisely  $\mu' - \mu < 0$  (or  $\sigma' - \sigma < 0$ ) then
        Fix sampling interval as  $(-\infty, 0]$  for  $\epsilon_\mu$  (or  $\epsilon_\sigma$ );
      else if channel-wisely  $\mu' - \mu > 0$  (or  $\sigma' - \sigma > 0$ ) then
        Fix sampling interval as  $[0, \infty)$  for  $\epsilon_\mu$  (or  $\epsilon_\sigma$ );
      else
        Fix sampling interval as  $(-\infty, \infty)$  for  $\epsilon_\mu$  (or  $\epsilon_\sigma$ );
      end if
      Resample  $\hat{\mu}'$  and  $\hat{\sigma}'$  for each  $\mathbf{z}'$  via Eq. (8);
      Reconstruct each  $\hat{\mathbf{z}}'$  via Eq. (9);
      Propagate the feature maps to the subsequent layer;
    end if
    Back-propagate to update  $\theta$  via gradient descent based on the batch of  $\mathbf{x}$ ,  $\mathbf{x}'$  and  $\hat{\mathbf{x}}'$ ;
  end for
end for
return Updated model  $F_\theta$ .
    
```

make false predictions. The FSU module reconstructs such points with larger variances. This process, to some extent, mitigates the influence of adversarial perturbations.

3.4. FSU for Testing or Model Fine-tuning

Models learned by natural training are not robust enough against powerful attacks. Especially, the feature statistics (μ, σ) are low-dimensional representations of examples, which in fact cause information loss of latent features. When confronted with powerful attacks, e.g., (Carlini & Wagner, 2017; Croce & Hein, 2020), the robustness decreases dramatically. We propose two solutions for this problem:

- **Solution 1:** Selecting a robust model established by adversarial training and directly incorporating FSU into the testing phase (including attacking and predicting).
- **Solution 2:** Fine-tuning a well-established model with FSU by introducing some directional information at the feature statistic-level, which achieves an effect similar to increasing attack strength in fine-tuning. The reconstructed examples are used as augmented data for parameter updating during each fine-tuning epoch.

The details of solution 2 are described in Algorithm 1. Note that both solution 1 and solution 2 can be realized on any well-established models.

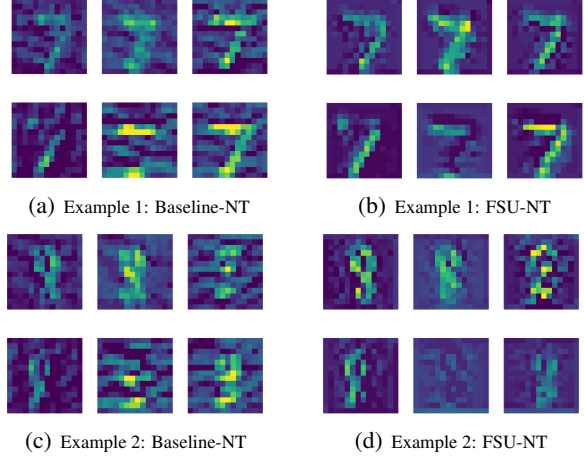


Figure 5. Feature maps of six channels for randomly selected testing examples in MNIST attacked by FGSM (with LeNet-5).

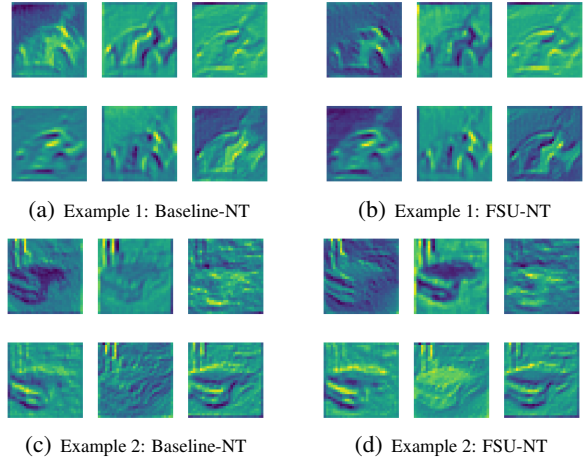


Figure 6. Feature maps of six randomly selected channels for randomly selected testing examples in CIFAR10 attacked by FGSM (with ResNet-18).

4. Experiments

Datasets We evaluate model robustness on datasets MNIST (LeCun et al., 1998), CIFAR10 (Krizhevsky et al., 2009), SVHN (Goodfellow et al., 2014) and CIFAR100 (Krizhevsky et al., 2009). Details on the datasets are provided in Appendix E.

Evaluation Protocols Both white-box and black-box attacks are performed. For white-box, we adopt the fast gradient sign method (FGSM) (Goodfellow et al., 2015), basic iterative method (BIM) (Kurakin et al., 2017), momentum-based iterative method (MIM) (Dong et al., 2018), projected gradient descent (PGD) (Madry et al., 2018) attack, auto attack (AA) (Croce & Hein, 2020) and Carlini & Wagner’s attack (CW) (Carlini & Wagner, 2017); for black-box, we adopt single-pixel attack (SPA) (Narodytska & Kasiviswanathan, 2016) and one-pixel attack (OPA) (Su et al., 2019). Among them, FGSM, BIM, MIM, PGD and AA are

Table 1. Robustness evaluation (%) (left part) and proportion of decision changes due to feature reconstruction (right part) of the proposed FSU method on datasets MNIST, CIFAR10, SVHN and CIFAR100.

Dataset	Method	Clean	FGSM	BIM	MIM	PGD	#Epochs / Time	P	Clean	FGSM	BIM	MIM	PGD
MNIST ($\epsilon = 0.3$)	Baseline-NT	99.20	13.59	0.69	0.69	0.67	100 / 944s	P_1 (%)	0.71	81.76	92.44	88.08	89.83
	FSU-NT	99.16±0.04	90.57±1.18	90.02±0.76	81.57±1.99	82.83±1.63	100 / 1306s	P_2 (%)	47.89	94.91	96.97	93.59	93.77
CIFAR10 ($\epsilon = 8/255$)	Baseline-NT	92.24	15.56	5.39	5.40	5.27	200 / 6826s	P_1 (%)	7.68	78.68	82.97	84.68	82.04
	FSU-NT	91.56±0.24	81.05±0.40	71.80±1.10	73.12±0.75	68.98±0.84	200 / 7152s	P_2 (%)	40.63	87.30	83.28	84.20	81.30
SVHN ($\epsilon = 8/255$)	Baseline-NT	96.09	34.38	5.67	7.10	8.84	100 / 4715s	P_1 (%)	3.00	60.8	84.92	84.40	81.73
	FSU-NT	96.14±0.09	84.11±0.54	79.14±0.66	78.72±0.75	78.07±0.97	100 / 4985s	P_2 (%)	41.43	86.39	88.33	87.37	87.42
CIFAR100 ($\epsilon = 8/255$)	Baseline-NT	74.01	16.16	9.06	9.32	8.32	300 / 10790s	P_1 (%)	22.77	75.72	80.96	81.81	78.24
	FSU-NT	72.96±0.17	43.51±0.46	41.69±0.53	43.43±0.63	37.00±0.71	300 / 11026s	P_2 (%)	26.88	44.32	47.90	49.79	43.98

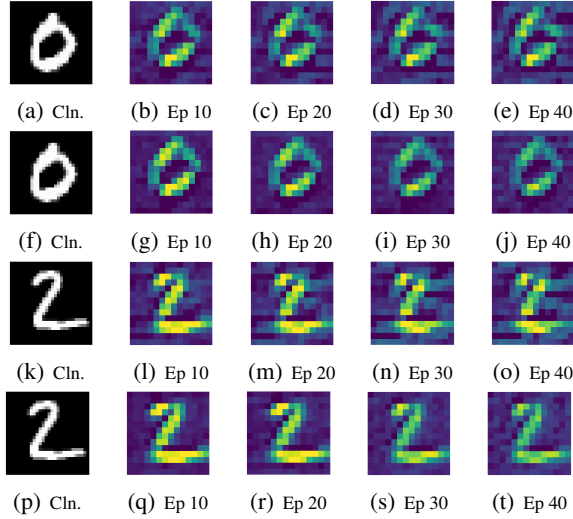


Figure 7. Feature maps of a randomly selected channel for randomly selected testing examples in MNIST during PGD-40 attack (with LeNet-5). (a)~(e) Example 1: Baseline-NT. (f)~(j) Example 1: FSU-NT. (k)~(o) Example 2: Baseline-NT. (p)~(t) Example 2: FSU-NT. (Ep means Epoch.)

l_∞ -bounded, OPA is l_0 -bounded, and CW is l_2 -bounded. Especially, for CW, the powerful optimization-based version with binary search is employed. The attack strength is set as $\epsilon = 0.3$ for MNIST and set as $\epsilon = 8/255$ for CIFAR10, SVHN and CIFAR100.

Platform The experiments are realized using python language with pytorch framework and advtorch library (Ding et al., 2019), conducted on a GeForce RTX 2080ti GPU with CUDA 10.1 and Ubuntu 16.04.

4.1. Natural Training for Typical Gradient Attacks

Backbones and Parameters In this section, a pure backbone DNN model is learned by natural training for each dataset, where the classic softmax cross-entropy loss is employed. LeNet-5 is used for MNIST; while ResNet-18 is used for CIFAR10, SVHN and CIFAR100. The FSU module is employed in both training and testing (including attacking and predicting) phases with $\alpha = \beta = 1$. In training, adaptive moment estimation (Adam) is used for optimization, with an initial learning rate 0.001, a cosine decay period 100, a minimum learning rate 10^{-6} , and a batch size of 128.

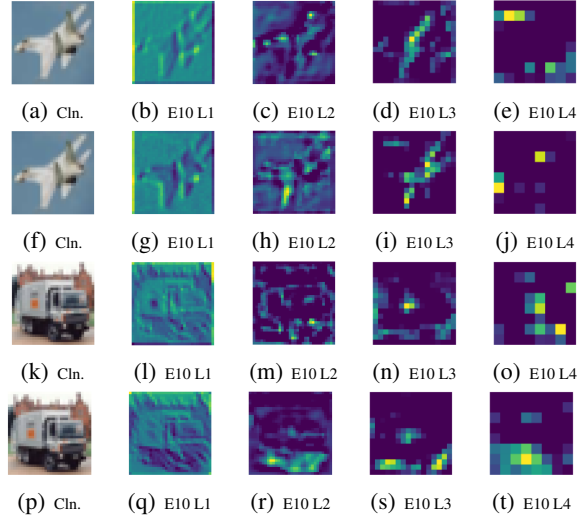


Figure 8. Feature maps of a randomly selected channel for randomly selected testing examples in CIFAR10 by PGD-10 attack (with ResNet-18). (a)~(e) Example 1: Baseline-NT. (f)~(j) Example 1: FSU-NT. (k)~(o) Example 2: Baseline-NT. (p)~(t) Example 2: FSU-NT. (E and L mean epoch and location. L1: after the first convolution layer; L2: after the first convolution block; L3: after the second convolution block; L4: after the third convolution block.)

The numbers of training epochs for the four datasets are 100, 200, 100 and 300, respectively. In testing, the examples are tested batch-by-batch, and the batch size is 1000. Typical FGSM, BIM, MIM and PGD attacks are performed. The number of attacking iterations for BIM, MIM and PGD is 40 (with step size 0.01) for MNIST, and 10 (with step size $\epsilon/10$) for CIFAR10, SVHN and CIFAR100.

Overall Performance Table 1 reports the clean accuracy, robust accuracy and time cost of natural training without FSU (Baseline-NT) and with FSU (FSU-NT). Obviously, the robustness has been significantly improved by FSU under all attacks. More importantly, the time cost of FSU is substantially the same as the baseline, which is much more efficient than existing mainstream defense methods. Furthermore, the right part of Table 1 reports the proportion of examples with decision change caused by FSU (P_1) and the proportion of examples in P_1 with decision change from wrong to correct (P_2). For clean examples, P_1 is very small, indicating that the FSU module has trivial impacts on clean

Table 2. Robustness comparison (%) under typical gradient-based white-box attacks.

Method	AT	Cln.	FGSM	BIM	MIM	PGD	Avg.	Time
CIFAR10 ($\epsilon = 8/255$)								
PCL (ICCV'19)	✓	89.9	59.2	36.8	37.6	30.2	50.7	187194s
TRADES (ICML'19)	✓	85.8	68.8	64.4	66.1	70.8	71.2	160872s
AT-AWP (NeurIPS'20)	✓	84.8	58.9	55.2	56.5	63.3	63.7	210223s
MAIL-TRADES (NeurIPS'21)	✓	84.0	56.0	52.9	53.8	60.8	61.5	101026s
MLCAT _{WP} (ICML'22)	✓	85.1	58.9	57.7	57.8	66.0	65.1	429540s
WB-SNN* (ICME'23)	✗	93.3	71.1	—	—	64.3	—	—
S-SNN* (ICME'23)	✗	93.3	72.4	—	—	65.1	—	—
AT+RiFT (ICCV'23)	✓	75.6	51.4	47.4	48.9	55.1	55.7	127665s
SAM (ICML'24)	✓	93.9	45.2	27.6	27.0	29.1	44.6	6496s
FSU-NT (Ours)	✗	91.6	81.1	70.8	73.1	69.0	77.1	7152s
SVHN ($\epsilon = 8/255$)								
PCL (ICCV'19)	✓	95.9	76.1	44.3	47.9	39.9	60.8	273098s
TRADES (ICML'19)	✓	91.7	74.0	66.8	68.3	74.3	75.0	243508s
AT-AWP (NeurIPS'20)	✓	93.4	66.6	71.3	60.5	62.8	70.9	112945s
MAIL-TRADES (NeurIPS'21)	✓	92.4	70.7	65.0	64.6	71.0	72.7	60007s
AT+RiFT (ICCV'23)	✓	91.2	60.7	53.9	56.3	62.4	64.9	75817s
DM-I-AT (ICML'23)	✓	95.6	79.5	74.0	75.1	80.6	80.9	—
FSU-NT (Ours)	✗	96.1	84.1	79.1	78.7	78.1	83.2	4985s
CIFAR100 ($\epsilon = 8/255$)								
TRADES (ICML'19)	✓	58.9	33.6	32.2	32.5	37.8	39.0	163013s
AT-AWP (NeurIPS'20)	✓	53.6	32.7	31.7	32.0	36.9	37.4	77060s
MAIL-TRADES (NeurIPS'21)	✓	61.3	31.3	29.0	29.8	35.7	37.4	114857s
MLCAT _{WP} (ICML'22)	✓	63.5	33.7	31.3	32.2	37.7	39.7	158484s
WB-SNN* (ICME'23)	✗	69.0	35.6	—	—	25.5	—	—
S-SNN* (ICME'23)	✗	69.8	40.9	—	—	33.5	—	—
AT+RiFT (ICCV'23)	✓	43.4	29.8	28.1	28.7	32.6	32.5	125939s
SAM (ICML'24)	✓	77.4	32.7	17.9	20.4	20.4	33.8	6566s
FSU-NT (Ours)	✗	73.0	43.5	41.7	43.4	37.0	47.7	11026s

Note: The results of methods marked with * are cited from the original papers; the well-trained model of DM-I-AT is downloaded for testing; all the other models are trained (under default parameter settings with recommended backbones) together with the proposed method.

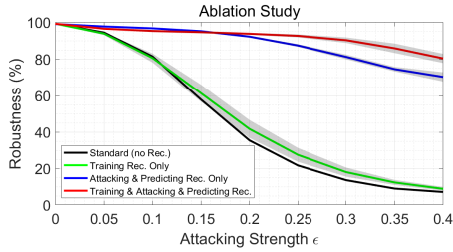


Figure 9. Robust accuracy on MNIST under FGSM attack when employing FSU in different stages (with LeNet-5).

examples. However, for attacked examples, the value of P_1 under all attacks is large. Moreover, the proportion of decisions changed from wrong to correct (i.e., P_2) is above 80% for MNIST, CIFAR10 and SVHN, i.e., batch-level statistics successfully helped many examples resist the attacks.

Visualization of Reconstructed Features Figs. 5~6 and Figs. 7~8 demonstrate the multi-channel feature maps of randomly selected testing examples attacked by FGSM and PGD, respectively. Note that Figs. 5 and 7 are for MNIST, and Figs. 6 and 8 are for CIFAR10. It can be seen that the FSU module does help the attacked examples recover some important feature points. Comparing to the feature maps obtained from the baseline model, the ones obtained from the FSU model have more clearer semantic information. In other words, the FSU module mitigates the influence of adversarial perturbations and weakens the ability of the attacks to deceive models.

Ablation Study Fig. 9 shows the robust accuracy against FGSM attack on MNIST in the cases of employing the FSU module in different stages. It can be observed that employing FSU only in training has similar accuracy with the baseline. This is a rational phenomenon, since no adver-

Table 3. Robustness comparison (%) under optimization-based black-box/white-box attacks.

Method	Cln.	SPA ₂₅	SPA ₅₀	SPA ₇₅	SPA ₁₀₀	OPA ₁	OPA ₂	OPA ₃	OPA ₅	CW ₂
MNIST ($\epsilon = 0.3$)										
TRADES	99.5	99.0	98.8	98.7	98.7	98.8	98.7	98.1	96.6	97.4
TRADES+FSU	99.2	99.3	99.3	99.4	99.3	99.0	99.1	98.8	98.2	99.4
AT-AWP	99.4	98.9	98.9	98.8	98.7	98.9	98.8	98.3	97.2	95.0
AT-AWP+FSU	99.2	99.2	99.2	99.2	99.3	98.9	98.8	98.7	98.2	99.0
MAIL-TRADES	99.1	96.7	96.6	93.7	88.7	97.9	97.4	97.0	96.5	51.7
MAIL-TRADES+FSU	99.1	98.3	98.2	97.3	95.2	99.1	99.1	99.1	99.1	62.7
MLCAT _{WP}	99.4	99.1	99.0	98.9	98.9	99.0	98.9	98.4	98.4	93.6
MLCAT _{WP} +FSU	99.3	99.3	99.3	99.4	99.4	99.1	99.1	98.9	98.9	99.1
CIFAR10 ($\epsilon = 8/255$)										
TRADES	85.8	77.9	76.4	75.7	75.2	77.9	75.5	72.1	68.4	0.4
TRADES+FSU	85.1	84.7	84.8	84.8	84.9	81.2	79.6	77.7	74.6	63.8
AT-AWP	84.8	78.2	77.0	76.5	76.2	79.7	78.3	75.9	73.4	0.1
AT-AWP+FSU	84.5	84.6	84.2	84.5	84.1	82.1	81.0	79.7	77.4	81.0
MAIL-TRADES	84.0	78.5	76.9	74.4	71.8	78.4	77.1	76.6	76.2	0.1
MAIL-TRADES+FSU	83.0	80.4	79.0	77.7	75.4	82.6	82.9	82.8	82.9	79.8
MLCAT _{WP}	85.1	78.7	77.5	76.9	76.5	80.7	79.0	77.4	75.2	0.5
MLCAT _{WP} +FSU	84.5	84.0	84.4	84.0	84.0	82.3	81.2	80.0	80.7	83.7
SVHN ($\epsilon = 8/255$)										
TRADES	91.7	88.1	86.9	86.1	85.6	88.3	87.3	85.1	82.6	0.1
TRADES+FSU	89.2	89.3	89.2	89.2	89.2	87.6	87.0	85.9	84.5	75.3
AT-AWP	93.4	89.0	87.2	86.2	85.4	88.7	86.8	83.4	79.2	0.1
AT-AWP+FSU	93.9	93.2	93.1	93.1	93.2	91.6	90.8	89.2	86.7	79.7
MAIL-TRADES	92.4	89.1	87.9	85.4	82.4	89.4	88.0	87.3	86.7	0.1
MAIL-TRADES+FSU	91.9	90.8	90.1	89.2	87.3	91.9	92.1	91.8	91.8	80.5
CIFAR100 ($\epsilon = 8/255$)										
TRADES	58.9	49.3	47.5	46.9	46.4	50.1	47.4	43.7	40.1	0.3
TRADES+FSU	54.4	54.4	54.1	54.5	54.4	50.8	49.1	47.0	43.9	54.3
AT-AWP	53.6	49.1	48.5	48.2	48.0	48.1	46.4	44.0	41.5	0.1
AT-AWP+FSU	50.5	49.6	50.2	49.9	49.8	47.0	46.1	44.9	43.0	50.0
MAIL-TRADES	92.4	52.6	50.1	46.4	42.8	52.7	51.7	51.1	50.8	0.1
MAIL-TRADES+FSU	91.9	55.3	53.9	51.6	49.1	59.3	59.2	59.3	59.6	58.4
MLCAT _{WP}	63.5	53.5	51.8	51.2	50.8	55.3	52.8	49.9	46.1	0.1
MLCAT _{WP} +FSU	58.8	58.8	58.6	58.8	58.7	55.9	54.5	52.8	49.7	59.0

Note: ● / ○ means that the robust accuracy is improved / not improved by incorporating the FSU module.

arial information is introduced during training, the reconstruction of clean training data has trivial impacts on test robustness. Despite this, employing FSU in training, attacking and predicting phases shows a significant improvement. As aforementioned, in training, FSU encourages the network to learn some uncertainty via Gaussian noise; while in testing, FSU reconstructs features in each epoch of attacking to recover some domain characteristics for classification.

Comparison with State-of-the-Art Methods We further compare the FSU method with recent state-of-the-art defense methods in Table 2, including PCL (Mustafa et al., 2019), TRADES (Zhang et al., 2019), AT-AWP (Wu et al., 2020), MAIL-TRADES (Wang et al., 2021), MLCAT_{WP} (Yu et al., 2022), AT+RiFT (Zhu et al., 2023), WB-SNN (Yang et al., 2023b), S-SNN (Yang et al., 2023a), DM-I-AT (Wang et al., 2023) and SAM (Zhang et al., 2024), where the results of FSU are the average of 10 trials. It can be seen that FSU did not sacrifice much accuracy on clean data; at the same time, it shows state-of-the-art performance under many attacks on CIFAR10, SVHN and CIFAR100. In addition, from the last column of Table 2, we know that the training cost of FSU is only about one tenth of the others. The second column of Table 2 indicates whether or not the method relies on adversarial training. A broad understanding is that adversarial training can effectively improve the model robustness, but it involves a large number of optimization iterations to generate perturbations, which is very computationally expensive. From this perspective, FSU achieves significant robustness improvement at almost no additional time cost.

4.2. Adversarial Training for Powerful Attacks

Models The DNN models learned by natural training are not robust enough against powerful attacks. We further select several robust models established by adversarial training (i.e., TRADES, AT-AWP, MAIL-TRADES and MLCAT_{WP} in Table 2) and incorporate the FSU module into the attacking and predicting phases of these models (solution 1), or fine-tune the models by FSU (solution 2).

Attacking Optimization-based white-box CW_2 , black-box SPA and OPA, as well as gradient-based large-step PGD_∞ and ensemble AA_∞ are performed. For SPA, the maximum number of pixels to perturb is set to 25, 50, 75, 100; for OPA, the number of pixels to change is set to 1, 2, 3, 5. CW attack has a confidence 0, the maximum number of iterations 1000, an initial constant 0.001, binary search steps 9, a learning rate 0.01 for MNIST and $5e-4$ for CIFAR10, SVHN and CIFAR100. For PGD, the attacking step size is $\epsilon/10$.

Robustness Improvement (Optimization-based Attacks)

Table 3 reports the robust accuracies of the several well-established models under the optimization-based SPA, OPA and CW attacks, as well as the accuracies by incorporating the FSU module (with $\alpha = \beta = 1$) into the attacking and predicting phases of these models. Obviously, the FSU module helps these models better defend against almost all of these attacks. Especially, the improvement under CW attack is remarkable. It is noteworthy that for CW we employ the original optimization-based version that implements the binary search, which is a very powerful attack. As can be seen from the last column of Table 3, these models all collapse on datasets CIFAR10, SVHN and CIFAR100 when facing CW attack. With the help of the FSU module, the robust accuracy improves to a great extent at almost no additional cost. Besides, it can even slightly exceed the clean accuracy, which is a phenomenon worth investigating in the future.

Calibration for Distribution Shifts Fig. 10 demonstrates the distributions of feature mean and standard deviation, i.e., (μ, σ) , of clean and CW-attacked testing examples in CIFAR10 induced by MLCAT_{WP} and $\text{MLCAT}_{\text{WP}}+\text{FSU}$. Obviously, the distribution shifts of both feature mean and standard deviation have been calibrated to a great extent by employing the FSU module.

Robustness Improvement (Large-Step PGD) We further select the MAIL-TRADES model and fine-tune it by Algorithm 1 with different parameter combinations of (α, β) , denoted as MAIL-TRADES+FSU-FiT. The number of fine-tuning epochs is set as 20. Table 4 reports the robust accuracies of this model and the fine-tuned models under the attacks of large-step PGD and AA on CIFAR10. Obviously, the robustness under large-step PGD attacks has been improved with almost all the parameter combinations. Besides, the performance is sensitive to α (i.e., the noise intensity of

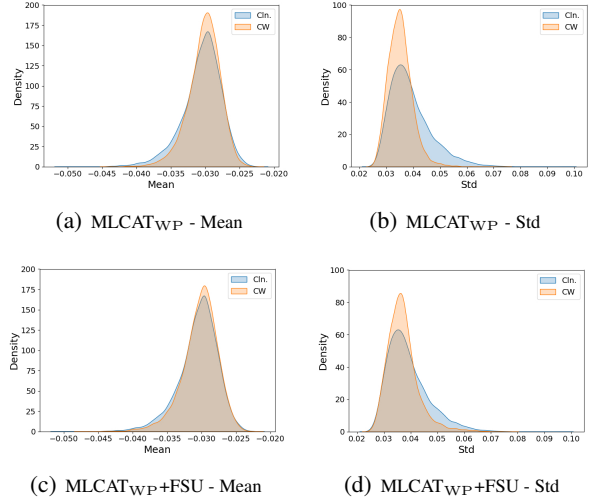


Figure 10. Distribution shifts of feature statistics (testing examples of CIFAR10 under CW attack).

Table 4. Robustness comparison (%) under PGD-20, PGD-40, PGD-100 and AA on CIFAR10.

Method	(α, β)	Cln.	PGD-20	PGD-40	PGD-100	AA
MAIL-TRADES	—	84.03	51.53	50.60	50.43	46.82
MAIL-TRADES+FSU-FiT	(0.1, 1.0)	83.54◦	51.99●	50.90●	50.68●	47.07●
MAIL-TRADES+FSU-FiT	(0.3, 0.4)	83.88◦	52.50●	51.30●	51.22●	47.02●
MAIL-TRADES+FSU-FiT	(0.3, 0.6)	83.75◦	52.24●	51.23●	51.06●	46.96●
MAIL-TRADES+FSU-FiT	(0.3, 0.8)	83.74◦	52.41●	51.38●	51.15●	46.92●
MAIL-TRADES+FSU-FiT	(0.3, 1.0)	83.01◦	52.59●	51.54●	51.37●	47.10●
MAIL-TRADES+FSU-FiT	(0.3, 1.2)	83.64◦	52.36●	51.41●	51.15●	47.04●
MAIL-TRADES+FSU-FiT	(0.3, 1.4)	83.78◦	52.42●	51.34●	51.14●	46.87●
MAIL-TRADES+FSU-FiT	(0.5, 0.4)	84.11●	52.56●	51.37●	51.14●	46.28◦
MAIL-TRADES+FSU-FiT	(0.5, 0.6)	83.99◦	52.70●	51.62●	51.30●	46.68◦
MAIL-TRADES+FSU-FiT	(0.5, 0.8)	83.95◦	52.64●	51.34●	51.25●	46.56◦
MAIL-TRADES+FSU-FiT	(0.5, 1.0)	82.87◦	52.81●	51.95●	51.72●	46.98●
MAIL-TRADES+FSU-FiT	(0.5, 1.2)	84.00●	52.53●	51.51●	51.31●	46.58◦
MAIL-TRADES+FSU-FiT	(0.5, 1.4)	83.91◦	52.59●	51.42●	51.19●	46.54◦
MAIL-TRADES+FSU-FiT	(0.7, 1.0)	83.49◦	53.02●	51.83●	51.54●	45.98◦
MAIL-TRADES+FSU-FiT	(0.9, 1.0)	83.71◦	52.33●	51.25●	51.06●	45.41◦

Note: ● / ◦ means that the robust accuracy is improved / not improved by incorporating the FSU module.

feature mean), while it is relatively stable with respect to β (i.e., the noise intensity of feature standard deviation).

Limitations Unfortunately, the robustness improvement of the fine-tuned models against AA is very limited. It is well-known that AA is a powerful ensemble attack that performs Auto-PGD_{CE}, Auto-PGD_{DLR}, fast boundary attack (FAB) and square attack sequentially. Among them, Auto-PGD_{DLR} is a targeted attack that attempts to disturb an example along the direction of each false class. As aforementioned, the feature statistics (μ, σ) can be seen as low-dimensional representations of examples, which in fact lose the directional information of features in latent space. From this perspective, the FSU module has limitations when facing targeted attacks, while it is universally effective when facing un-targeted ones.

Appendices More technical details about the experimental configurations, random seeds, results visualizations, etc., are provided in Appendix F. Descriptions on the codes and models are provided in Appendix G.

5. Conclusion

We enhance the adversarial robustness of DNNs by reconstructing feature maps based on channel-wise statistical feature mean and standard deviation of a batch of examples. Gaussian noise is used to model the uncertainty of the statistical feature mean and standard deviation, which mitigates the influence of the perturbations from attackers, and helps the reconstructed feature maps recover some domain characteristics for classification. The proposed module does not rely on adversarial information, it can be universally applied to natural training, adversarial training, attacking, predicting, and model fine-tuning for robustness enhancement, which achieves promising improvements against various attacks with trivial additional time cost.

Impact Statement

This paper presents work whose goal is to advance the field of Machine Learning. There are many potential societal consequences of our work, none which we feel must be specifically highlighted here.

References

- Alemi, A. A., Fischer, I., Dillon, J. V., and Murphy, K. Deep variational information bottleneck. In *International Conference on Learning Representations*, 2017.
- Carbone, G., Wicker, M., Laurenti, L., Patane', A., Bor-tolussi, L., and Sanguinetti, G. Robustness of bayesian neural networks to gradient-based attacks. In *Advances in Neural Information Processing Systems*, 2020.
- Carlini, N. and Wagner, D. Towards evaluating the robustness of neural networks. In *IEEE Symposium on Security and Privacy*, pp. 39–57, 2017.
- Cohen, J., Rosenfeld, E., and Kolter, Z. Certified adversarial robustness via randomized smoothing. In *International Conference on Machine Learning*, pp. 1310–1320, 2019.
- Croce, F. and Hein, M. Reliable evaluation of adversarial robustness with an ensemble of diverse parameter-free attacks. In *International Conference on Machine Learning*, 2020.
- Ding, G. W., Wang, L., and Jin, X. Advtorch v0. 1: An adversarial robustness toolbox based on pytorch. *arXiv preprint arXiv:1902.07623*, 2019.
- Dong, Y., Liao, F., Pang, T., Su, H., Zhu, J., Hu, X., and Li, J. Boosting adversarial attacks with momentum. In *IEEE/CVF Conference on Computer Vision and Pattern Recognition*, pp. 9185–9193, 2018.
- Eustratiadis, P., Gouk, H., Li, D., and Hospedales, T. Weight-covariance alignment for adversarially robust neural networks. In *International Conference on Machine Learning*, pp. 3047–3056, 2021.
- Goodfellow, I., Ibarz, J., Bulatov, Y., Arnoud, S., and Shet, V. Multi-digit number recognition from street view imagery using deep convolutional neural networks. In *International Conference on Learning Representations*, 2014.
- Goodfellow, I. J., Shlens, J., and Szegedy, C. Explaining and harnessing adversarial examples. In *International Conference on Learning Representations*, San Diego, CA, USA, 2015.
- He, Z., Rakin, A. S., and Fan, D. Parametric noise injection: Trainable randomness to improve deep neural network robustness against adversarial attack. In *IEEE/CVF Conference on Computer Vision and Pattern Recognition*, pp. 588–597, 2019.
- Jeddi, A., Shafiee, M. J., Karg, M., Scharfenberger, C., and Wong, A. Learn2perturb: an end-to-end feature perturbation learning to improve adversarial robustness. In *IEEE/CVF Conference on Computer Vision and Pattern Recognition*, pp. 1241–1250, 2020.
- Krizhevsky, A., Hinton, G., et al. Learning multiple layers of features from tiny images. *Handbook of Systemic Autoimmune Diseases*, 1(4), 2009.
- Kurakin, A., Goodfellow, I. J., and Bengio, S. Adversarial machine learning at scale. In *International Conference on Learning Representations*, 2017.
- LeCun, Y., Bottou, L., Bengio, Y., and Haffner, P. Gradient-based learning applied to document recognition. *Proceedings of the IEEE*, 86(11):2278–2324, 1998.
- Li, B., Chen, C., Wang, W., and Carin, L. Certified adversarial robustness with additive noise. *Advances in Neural Information Processing Systems*, 32, 2019.
- Li, X., Dai, Y., Ge, Y., Liu, J., Shan, Y., and Duan, L.-Y. Uncertainty modeling for out-of-distribution generalization. In *International Conference on Learning Representations*, 2022.
- Liu, X., Cheng, M., Zhang, H., and Hsieh, C.-J. Towards robust neural networks via random self-ensemble. In *European Conference on Computer Vision*, pp. 369–385, 2018a.
- Liu, X., Li, Y., Wu, C., and Hsieh, C.-J. Adv-bnn: Improved adversarial defense through robust bayesian neural network. In *International Conference on Learning Representations*, 2018b.

- Madry, A., Makelov, A., Schmidt, L., Tsipras, D., and Vladu, A. Towards deep learning models resistant to adversarial attacks. In *International Conference on Learning Representations*, 2018.
- Mustafa, A., Khan, S., Hayat, M., Goecke, R., Shen, J., and Shao, L. Adversarial defense by restricting the hidden space of deep neural networks. In *IEEE/CVF International Conference on Computer Vision*, pp. 3385–3394, 2019.
- Narodytska, N. and Kasiviswanathan, S. P. Simple black-box adversarial perturbations for deep networks. *arXiv:1612.06299*, 2016.
- Shafahi, A., Najibi, M., Ghiasi, M. A., Xu, Z., Dickerson, J., Studer, C., Davis, L. S., Taylor, G., and Goldstein, T. Adversarial training for free! *Advances in Neural Information Processing Systems*, 32, 2019.
- Su, J., Vargas, D. V., and Sakurai, K. One pixel attack for fooling deep neural networks. *IEEE Transactions on Evolutionary Computation*, 23(5):828–841, 2019.
- Szegedy, C., Zaremba, W., Sutskever, I., Bruna, J., Erhan, D., Goodfellow, I., and Fergus, R. Intriguing properties of neural networks. In *International Conference on Learning Representations*, 2014.
- Wang, Q., Liu, F., Han, B., and et al. Probabilistic margins for instance reweighting in adversarial training. In *Advances in Neural Information Processing Systems*, 2021.
- Wang, R., Ke, H., Hu, M., and Wu, W. Adversarially robust neural networks with feature uncertainty learning and label embedding. *Neural Networks*, 172(106087), 2024.
- Wang, Y., Zou, D., Yi, J., Bailey, J., Ma, X., and Gu, Q. Improving adversarial robustness requires revisiting misclassified examples. In *International Conference on Learning Representations*, 2020.
- Wang, Z., Pang, T., Du, C., Lin, M., Liu, W., and Yan, S. Better diffusion models further improve adversarial training. In *International Conference on Machine Learning*, 2023.
- Wu, D., Xia, S. T., and Wang, Y. Adversarial weight perturbation helps robust generalization. In *Advances in Neural Information Processing Systems*, 2020.
- Xie, C., Wang, J., Zhang, Z., Ren, Z., and Yuille, A. Mitigating adversarial effects through randomization. In *International Conference on Learning Representations*, 2018.
- Yang, H., Wang, M., Yu, Z., and Zhou, Y. A simple stochastic neural network for improving adversarial robustness. In *IEEE International Conference on Multimedia and Expo*, pp. 2297–2302, 2023a.
- Yang, H., Wang, M., Yu, Z., and Zhou, Y. Weight-based regularization for improving robustness in image classification. In *IEEE International Conference on Multimedia and Expo*, pp. 1775–1780, 2023b.
- Yu, C., Han, B., Shen, L., Yu, J., Gong, C., Gong, M., and Liu, T. Understanding robust overfitting of adversarial training and beyond. In *International Conference on Machine Learning*, 2022.
- Zhang, H., Yu, Y., Jiao, J., Xing, E., El Ghaoui, L., and Jordan, M. Theoretically principled trade-off between robustness and accuracy. In *International Conference on Machine Learning*, pp. 7472–7482, 2019.
- Zhang, Y., He, H., Zhu, J., Chen, H., Wang, Y., and Wei, Z. On the duality between sharpness-aware minimization and adversarial training. In *International Conference on Machine Learning*, 2024.
- Zhu, K., Hu, X., Wang, J., Xie, X., and Yang, G. Improving generalization of adversarial training via robust critical fine-tuning. In *International Conference on Computer Vision*, 2023.

A. Proof of Proposition 2.1

Lemma A.1. Let Ω be the convex hull of examples $\mathbf{x}_1, \mathbf{x}_2, \dots, \mathbf{x}_N$, then Ω can be covered by the weighted average of $\mathbf{x}_1, \mathbf{x}_2, \dots, \mathbf{x}_N$. That is, $\forall \mathbf{x} \in \Omega$, we can find a weight vector $\mathbf{w} = [w_1, w_2, \dots, w_N]$, $w_i \in [0, 1]$, $\sum_{i=1}^N w_i = 1$ such that $\mathbf{x} = \sum_{i=1}^N w_i \mathbf{x}_i$.

Proof. We prove it from the simplest case with three examples in two-dimensional space as shown in Fig. 11.

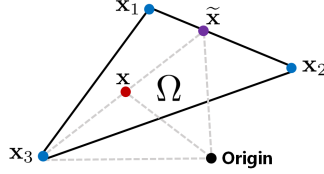


Figure 11. A case with three examples in two-dimensional space.

For any example \mathbf{x} in the convex hull of $\{\mathbf{x}_1, \mathbf{x}_2, \mathbf{x}_3\}$, i.e., $\forall \mathbf{x} \in \Omega(\mathbf{x}_1, \mathbf{x}_2, \mathbf{x}_3)$, we can find a line that crosses \mathbf{x} and \mathbf{x}_3 and intersects with $\mathbf{x}_1\mathbf{x}_2$ at $\tilde{\mathbf{x}}$. We can denote $\tilde{\mathbf{x}} = \alpha\mathbf{x}_1 + (1 - \alpha)\mathbf{x}_2$, where $\alpha \in [0, 1]$. Then,

$$\begin{aligned} \mathbf{x} &= \beta\tilde{\mathbf{x}} + (1 - \beta)\mathbf{x}_3 \\ &= \beta(\alpha\mathbf{x}_1 + (1 - \alpha)\mathbf{x}_2) + (1 - \beta)\mathbf{x}_3 \\ &= \beta\alpha\mathbf{x}_1 + \beta(1 - \alpha)\mathbf{x}_2 + (1 - \beta)\mathbf{x}_3 \\ &= w_1\mathbf{x}_1 + w_2\mathbf{x}_2 + w_3\mathbf{x}_3, \end{aligned}$$

where $\beta \in [0, 1]$, $w_1 = \beta\alpha$, $w_2 = \beta(1 - \alpha)$, $w_3 = 1 - \beta$, and

$$w_1 + w_2 + w_3 = \beta\alpha + \beta - \beta\alpha + 1 - \beta = 1.$$

This proof can be easily generalized to complex cases with more examples in higher dimensional space by mathematical induction. \square

Assumption A.2. Given a set of clean examples $\mathbf{x}_1, \mathbf{x}_2, \dots, \mathbf{x}_N$ and a classification model with certain robustness (e.g., a model trained by adversarial training), the corresponding adversarial examples $\mathbf{x}'_1, \mathbf{x}'_2, \dots, \mathbf{x}'_N$ will be in the convex hull of the clean examples, i.e., $\mathbf{x}'_1, \mathbf{x}'_2, \dots, \mathbf{x}'_N \in \Omega(\mathbf{x}_1, \mathbf{x}_2, \dots, \mathbf{x}_N)$.

Assumption A.2 means, according to Lemma A.1, each adversarial example can be represented as a weighted sum of the clean examples, i.e., $\mathbf{x}'_i = \sum_{j=1}^N w_{ij}\mathbf{x}_j$, where $w_{ij} \in [0, 1]$, $\sum_{j=1}^N w_{ij} = 1$, $i, j = 1, \dots, N$. This assumption intuitively holds with a high probability. As shown in the following Fig. 12, the attacking on an example is usually towards the decision boundary with another class. Along such direction, with an upper bound limit of the perturbation size ϵ , the adversarial example is still in the convex hull with a high probability.

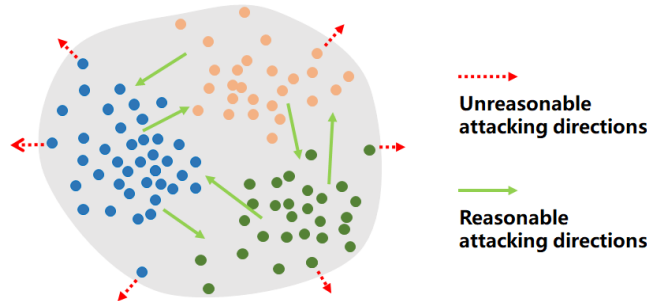


Figure 12. An intuitive illustration for Assumption A.2.

Lemma A.3. Let $\mathbf{W} = [\mathbf{w}_1; \mathbf{w}_2; \dots; \mathbf{w}_N] \in \mathcal{R}^{N \times N}$ be a weight matrix that satisfies

$$\begin{aligned} \mathbf{w}_i &= [w_{i,1}, w_{i,2}, \dots, w_{i,N}], \quad i = 1, \dots, N, \\ w_{i,j} &\in [0, 1), \quad i = 1, \dots, N, \quad j = 1, \dots, N, \\ \sum_{j=1}^N w_{i,j} &= 1, \quad i = 1, \dots, N, \\ \sum_{i=1}^N \sum_{j=1}^N w_{i,j} &= N. \end{aligned} \quad (13)$$

Denote $\mathbb{W} = \{\mathbf{W}\}$ as the set that contains all the weight matrices satisfying (13), then \mathbb{W} is closed with respect to multiplication.

Proof. For any $\mathbf{A}, \mathbf{B} \in \mathbb{W}$, denote $\mathbf{C} = \mathbf{BA}$. Obviously, there are

$$c_{i,j} = \sum_{k=1}^N a_{i,k} b_{k,j} \in [0, 1), \quad (14)$$

$$\sum_{j=1}^N c_{i,j} = \sum_{j=1}^N \sum_{k=1}^N a_{i,k} b_{k,j} = \sum_{k=1}^N a_{i,k} \sum_{j=1}^N b_{k,j} = 1 \times 1 = 1, \quad (15)$$

$$\sum_{i=1}^N \sum_{j=1}^N c_{i,j} = N. \quad (16)$$

Thus, $\mathbf{C} \in \mathbb{W}$. □

Lemma A.3 tells that after two attacking steps \mathbf{A} and \mathbf{B} , the attacked examples will be still in the convex hull of the clean examples.

Lemma A.4. Let $\mathbf{W}^1, \mathbf{W}^2, \dots, \mathbf{W}^t \in \mathbb{W}$ and $\mathbf{W}^{(t)} = \mathbf{W}^t \dots \mathbf{W}^2 \mathbf{W}^1$, when t is large enough, $\mathbf{W}^{(t)}$ will converge to a fixed matrix, and there is $w_{1,j}^{(t)} = w_{2,j}^{(t)} = \dots = w_{N,j}^{(t)}$, $j = 1, \dots, N$, i.e., the values in each column of $\mathbf{W}^{(t)}$ become equal.

Proof. Since $\mathbf{W}^{(t)} = \mathbf{W}^t \mathbf{W}^{(t-1)}$, there are

- $w_{i,j}^{(t)} = \sum_{k=1}^N w_{i,k}^t w_{k,j}^{(t-1)} \geq \min_k \{w_{k,j}^{(t-1)}\} \sum_{k=1}^N w_{i,k}^t = \min_k \{w_{k,j}^{(t-1)}\},$
- $w_{i,j}^{(t)} = \sum_{k=1}^N w_{i,k}^t w_{k,j}^{(t-1)} \leq \max_k \{w_{k,j}^{(t-1)}\} \sum_{k=1}^N w_{i,k}^t = \max_k \{w_{k,j}^{(t-1)}\}.$

Therefore $w_{i,j}^{(t)} \in [\min_k \{w_{k,j}^{(t-1)}\}, \max_k \{w_{k,j}^{(t-1)}\}]$, i.e., $[\min_i \{w_{i,j}^{(t)}\}, \max_i \{w_{i,j}^{(t)}\}] \subseteq [\min_k \{w_{k,j}^{(t-1)}\}, \max_k \{w_{k,j}^{(t-1)}\}]$, from which we know that $\min_i \{w_{i,j}^{(t)}\}$ is monotonically increasing with respect to t , and $\max_i \{w_{i,j}^{(t)}\}$ is monotonically decreasing with respect to t . Since $\min_i \{w_{i,j}^{(t)}\} < \max_i \{w_{i,j}^{(1)}\}$ and $\max_i \{w_{i,j}^{(t)}\} > \min_i \{w_{i,j}^{(1)}\}$, we know that $\min_i \{w_{i,j}^{(t)}\}$ has upper bound and $\max_i \{w_{i,j}^{(t)}\}$ has lower bound. According to the monotonic bounded theorem, both $\min_i \{w_{i,j}^{(t)}\}$ and $\max_i \{w_{i,j}^{(t)}\}$ converge with respect to t , therefore the mathematical limits of $\min_i \{w_{i,j}^{(t)}\}$ and $\max_i \{w_{i,j}^{(t)}\}$ exist.

Without loss of generality, suppose $\exists \xi_1 > \min_i \{w_{i,j}^{(1)}\}$ and $\exists \xi_2 < \max_i \{w_{i,j}^{(1)}\}$ such that $\lim_{t \rightarrow \infty} \min_i \{w_{i,j}^{(t)}\} = \xi_1$ and $\lim_{t \rightarrow \infty} \max_i \{w_{i,j}^{(t)}\} = \xi_2$. That is, $\forall \varepsilon > 0$,

- $\exists \lambda_1 \in \mathcal{R}, 0 < \lambda_1 < 1, \exists N_1 \in \mathbb{Z}^+$, such that when $t > N_1$ there is $|\min_i \{w_{i,j}^{(t)}\} - \xi_1| < \frac{\lambda_1 \varepsilon}{2}$,
- $\exists \lambda_2 \in \mathcal{R}, 0 < \lambda_2 < 1, \exists N_2 \in \mathbb{Z}^+$, such that when $t > N_2$ there is $|\max_i \{w_{i,j}^{(t)}\} - \xi_2| < \frac{\lambda_2 \varepsilon}{2}$.

Therefore, when $t > N_1 + N_2$,

$$\begin{aligned} |\min_i\{w_{i,j}^{(t)}\} - \min_i\{w_{i,j}^{(t+1)}\}| &= |(\min_i\{w_{i,j}^{(t)}\} - \xi_1) - (\min_i\{w_{i,j}^{(t+1)}\} - \xi_1)| \\ &\leq |\min_i\{w_{i,j}^{(t)}\} - \xi_1| + |\min_i\{w_{i,j}^{(t+1)}\} - \xi_1| \\ &< \lambda_1 \varepsilon, \end{aligned} \quad (17)$$

$$\begin{aligned} |\max_i\{w_{i,j}^{(t+1)}\} - \max_i\{w_{i,j}^{(t)}\}| &= |(\max_i\{w_{i,j}^{(t+1)}\} - \xi_2) - (\max_i\{w_{i,j}^{(t)}\} - \xi_2)| \\ &\leq |\max_i\{w_{i,j}^{(t+1)}\} - \xi_2| + |\max_i\{w_{i,j}^{(t)}\} - \xi_2| \\ &< \lambda_2 \varepsilon. \end{aligned} \quad (18)$$

Since $[\min_i\{w_{i,j}^{(t+1)}\}, \max_i\{w_{i,j}^{(t+1)}\}] \subseteq [\min_i\{w_{i,j}^{(t)}\}, \max_i\{w_{i,j}^{(t)}\}]$, we can denote

- $\min_i\{w_{i,j}^{(t+1)}\} = \lambda_1 \max_i\{w_{i,j}^{(t)}\} + (1 - \lambda_1) \min_i\{w_{i,j}^{(t)}\}$,
- $\max_i\{w_{i,j}^{(t+1)}\} = (1 - \lambda_2) \max_i\{w_{i,j}^{(t)}\} + \lambda_2 \min_i\{w_{i,j}^{(t)}\}$.

Therefore,

- $|\min_i\{w_{i,j}^{(t)}\} - \lambda_1 \max_i\{w_{i,j}^{(t)}\} - (1 - \lambda_1) \min_i\{w_{i,j}^{(t)}\}| < \lambda_1 \varepsilon$, thus $|\min_i\{w_{i,j}^{(t)}\} - \max_i\{w_{i,j}^{(t)}\}| < \varepsilon$,
- $|(1 - \lambda_2) \max_i\{w_{i,j}^{(t)}\} + \lambda_2 \min_i\{w_{i,j}^{(t)}\} - \max_i\{w_{i,j}^{(t)}\}| < \lambda_2 \varepsilon$, thus $|\max_i\{w_{i,j}^{(t)}\} - \min_i\{w_{i,j}^{(t)}\}| < \varepsilon$.

This means, when $t > N_1 + N_2$, $\forall \varepsilon > 0$ there is $|\xi_1 - \xi_2| < \varepsilon$, i.e., $\xi_1 = \xi_2 = \xi$, $\lim_{t \rightarrow \infty} \min_i\{w_{i,j}^{(t)}\} = \lim_{t \rightarrow \infty} \max_i\{w_{i,j}^{(t)}\} = \xi$.

Finally, we get the conclusion that when $t \rightarrow \infty$, there is $w_{1,j}^{(t)} = w_{2,j}^{(t)} = \dots = w_{N,j}^{(t)} = \xi$, i.e., the values in each column of $\mathbf{W}^{(t)}$ become equal. \square

Lemma A.4 tells the extreme case for adversarial attack that when the perturbation bound ϵ and the number of attacking steps t are large enough, all the examples will finally shrink to the same point. Of course, this extreme case will never happen, since in order to ensure the imperceptibility, the perturbation bound ϵ cannot be too large, and the number of attacking steps t cannot be infinite. However, **Lemma A.4** provides some guidelines for further theoretical analysis.

Proposition 2.1 Suppose the set of clean examples $\mathbf{x}_1, \mathbf{x}_2, \dots, \mathbf{x}_N$ are attacked into adversarial examples $\mathbf{x}'_1, \mathbf{x}'_2, \dots, \mathbf{x}'_N$ through a classification model. With a high probability, the variance of feature means becomes smaller after being attacked.

Proof. Let $\mathbf{x}_i = [x_{i1}, \dots, x_{id}]$ (which is a row vector) be the i -th clean example, and $\mathbf{X} = [\mathbf{x}_1; \dots; \mathbf{x}_N]$ be the clean data matrix. According to **Lemma A.1** and **Assumption A.2**, there are

$$\begin{aligned} \mathbf{x}'_1 &= w_{11}\mathbf{x}_1 + w_{12}\mathbf{x}_2 + \dots + w_{1N}\mathbf{x}_N = \mathbf{w}_1\mathbf{X} = [x'_{11}, \dots, x'_{1d}], \\ \mathbf{x}'_2 &= w_{21}\mathbf{x}_1 + w_{22}\mathbf{x}_2 + \dots + w_{2N}\mathbf{x}_N = \mathbf{w}_2\mathbf{X} = [x'_{21}, \dots, x'_{2d}], \\ &\dots \\ \mathbf{x}'_N &= w_{N1}\mathbf{x}_1 + w_{N2}\mathbf{x}_2 + \dots + w_{NN}\mathbf{x}_N = \mathbf{w}_N\mathbf{X} = [x'_{N1}, \dots, x'_{Nd}], \end{aligned} \quad (19)$$

where

$$\begin{aligned} \mathbf{w}_i &= [w_{i,1}, w_{i,2}, \dots, w_{i,N}], \quad i = 1, \dots, N, \\ w_{i,j} &\in [0, 1], \quad i = 1, \dots, N, \quad j = 1, \dots, N, \\ \sum_{j=1}^N w_{i,j} &= 1, \quad i = 1, \dots, N, \\ \sum_{i=1}^N \sum_{j=1}^N w_{i,j} &= N. \end{aligned} \quad (20)$$

Denote $\mathbf{W} = [\mathbf{w}_1; \mathbf{w}_2; \dots; \mathbf{w}_N]$, (19) can be re-written into the matrix form, i.e.,

$$\mathbf{X}' = \mathbf{W}\mathbf{X}. \quad (21)$$

Let $\alpha = [\frac{1}{d}, \frac{1}{d}, \dots, \frac{1}{d}]$, then for a clean example \mathbf{x}_i and its corresponding adversarial example \mathbf{x}'_i , their feature means are calculated as

$$\begin{aligned} \mu_i &= \frac{1}{d} \sum_{j=1}^d x_{ij} = \mathbf{x}_i \alpha^\top, \\ \mu'_i &= \frac{1}{d} \sum_{j=1}^d x'_{ij} = \mathbf{x}'_i \alpha^\top. \end{aligned} \quad (22)$$

Denote $\boldsymbol{\mu} = [\mu_1, \mu_2, \dots, \mu_N]^\top$ and $\boldsymbol{\mu}' = [\mu'_1, \mu'_2, \dots, \mu'_N]^\top$, there are

$$\begin{aligned}\boldsymbol{\mu} &= \mathbf{X}\boldsymbol{\alpha}^\top, \\ \boldsymbol{\mu}' &= \mathbf{X}'\boldsymbol{\alpha}^\top = \mathbf{W}\mathbf{X}\boldsymbol{\alpha}^\top = \mathbf{W}\boldsymbol{\mu}.\end{aligned}\quad (23)$$

Further let $\beta = [\frac{1}{N}, \frac{1}{N}, \dots, \frac{1}{N}]$, the expectaions of μ and μ' are estimated as

$$\begin{aligned}\mathbb{E}(\mu) &= \frac{1}{Nd} \sum_{i=1}^N \sum_{j=1}^d x_{ij} = \beta \mathbf{X}\boldsymbol{\alpha}^\top = \Phi_\mu, \\ \mathbb{E}(\mu') &= \frac{1}{Nd} \sum_{i=1}^N \sum_{j=1}^d x'_{ij} = \beta \mathbf{X}'\boldsymbol{\alpha}^\top = \beta \mathbf{W}\mathbf{X}\boldsymbol{\alpha}^\top = \Phi_{\mu'}.\end{aligned}\quad (24)$$

The variance of $\{\mu_1, \mu_2, \dots, \mu_N\}$ is estimated as

$$\text{var}(\mu) = \frac{1}{N} \sum_{i=1}^N (\mu_i - \Phi_\mu)^2 = \frac{1}{N} \sum_{i=1}^N (\mu_i^2 - 2\mu_i\Phi_\mu + \Phi_\mu^2) = \frac{1}{N} \sum_{i=1}^N (\mu_i^2 - \Phi_\mu^2) = \Sigma_\mu^2. \quad (25)$$

Similarly, the variance of $\{\mu'_1, \mu'_2, \dots, \mu'_N\}$ is estimated as

$$\text{var}(\mu') = \frac{1}{N} \sum_{i=1}^N ((\mu'_i)^2 - (\Phi_{\mu'})^2) = \Sigma_{\mu'}^2. \quad (26)$$

We reasonably assume that the adversarial attack didn't change the expectation of the feature means, i.e., $\Phi_\mu = \Phi_{\mu'}$, then the difference of the two variances is calculated as

$$\begin{aligned}\text{var}(\mu) - \text{var}(\mu') &= \frac{1}{N} \sum_{i=1}^N (\mu_i^2 - \Phi_\mu^2) - \frac{1}{N} \sum_{i=1}^N ((\mu'_i)^2 - (\Phi_{\mu'})^2) \\ &= \frac{1}{N} \sum_{i=1}^N \mu_i^2 - \frac{1}{N} \sum_{i=1}^N (\mu'_i)^2 \\ &= \frac{1}{N} \sum_{i=1}^N (\mu_i^2 - (\mu'_i)^2) \\ &= \frac{1}{N} (\boldsymbol{\mu}^\top \boldsymbol{\mu} - (\boldsymbol{\mu}')^\top (\boldsymbol{\mu}')) \\ &= \frac{1}{N} (\boldsymbol{\mu}^\top \boldsymbol{\mu} - \boldsymbol{\mu}^\top \mathbf{W}^\top \mathbf{W} \boldsymbol{\mu}) \\ &= \frac{1}{N} (\boldsymbol{\mu}^\top (\mathbf{I} - \mathbf{W}^\top \mathbf{W}) \boldsymbol{\mu}).\end{aligned}\quad (27)$$

Let $\mathbf{A} = \mathbf{W}^\top \mathbf{W}$ (\mathbf{A} is a real symmetric matrix), and perform orthogonal decomposition to \mathbf{A} , there is

$$\mathbf{A} = \mathbf{Q}\boldsymbol{\Lambda}\mathbf{Q}^\top, \quad (28)$$

where \mathbf{Q} is an orthogonal matrix, $\boldsymbol{\Lambda} = \text{diag}(\lambda_1, \lambda_2, \dots, \lambda_N)$, $\lambda_1 \geq \lambda_2 \geq \dots \geq \lambda_N \geq 0$ are the eigenvalues of \mathbf{A} and $\sum_{i=1}^N \lambda_i = \text{tr}(\mathbf{W}^\top \mathbf{W}) = \sum_{i=1}^N \sum_{j=1}^N w_{i,j}^2$. Furthermore, since $w_{i,j} \in [0, 1]$ and $\sum_{i=1}^N \sum_{j=1}^N w_{i,j} = N$, it is obvious that $\sum_{i=1}^N \lambda_i \leq N$. Let $\mathbf{z} = \mathbf{Q}^\top \boldsymbol{\mu} = [z_1, z_2, \dots, z_N]^\top$, then

$$\begin{aligned}\text{var}(\mu) - \text{var}(\mu') &= \frac{1}{N} (\mathbf{z}^\top \mathbf{Q}^\top \mathbf{Q} \mathbf{z} - \mathbf{z}^\top \boldsymbol{\Lambda} \mathbf{z}) \\ &= \frac{1}{N} (\mathbf{z}^\top \mathbf{z} - \mathbf{z}^\top \boldsymbol{\Lambda} \mathbf{z}) \\ &= \frac{1}{N} ((1 - \lambda_1)z_1^2 + (1 - \lambda_2)z_2^2 + \dots + (1 - \lambda_N)z_N^2).\end{aligned}\quad (29)$$

We discuss the situation that a series of attacking steps $\mathbf{W}^1, \mathbf{W}^2, \dots, \mathbf{W}^t$ finally lead to the attacking results, i.e.,

$$\mathbf{X}' = \mathbf{W}^t \dots \mathbf{W}^2 \mathbf{W}^1 \mathbf{X} = \mathbf{W}^{(t)} \mathbf{X}. \quad (30)$$

Suppose \mathbf{W}^1 is full rank. Based on traditional textbook, and according to **Lemma A.3** and **Lemma A.4**, when $t \rightarrow \infty$, there is

$$N = \text{rank}(\mathbf{W}^1) \geq \text{rank}(\mathbf{W}^2 \mathbf{W}^1) \geq \text{rank}(\mathbf{W}^3 \mathbf{W}^2 \mathbf{W}^1) \geq \dots \geq \text{rank}(\mathbf{W}^{(t)}) = 1. \quad (31)$$

For the extreme case of $t \rightarrow \infty$, it is obvious that $\text{var}(\mu) - \text{var}(\mu') > 0$ holds with probability 1. Correspondingly, from the initial state to the extreme state, the rank of $\mathbf{W}^{(t)}$ becomes smaller and smaller, i.e., the zero eigenvalues become more and more, thereby the must-positive terms in Eq. (29) become more and more. During this process, since $\sum_{i=1}^N \lambda_i \leq N$ always holds, we can say that $\text{var}(\mu) - \text{var}(\mu') \geq 0$ holds with a high probability. \square

Geometric Interpretation This ‘‘high probability’’ can be interpreted geometrically. From Eq. (27) we know that $\text{var}(\mu) - \text{var}(\mu') \geq 0$ holds when $\mu^\top \mu \geq \mu^\top \mathbf{W}^\top \mathbf{W} \mu$, i.e., $|\mu| \geq |\mathbf{W}\mu| = |\mu'|$. Taking the origin as the center and $|\mu|$ as the radius of a hypersphere in N -dimensional space, obviously, there are $|\mu| > |\mu'|$ when μ' is inside the hypersphere, and $|\mu| < |\mu'|$ when μ' is outside the hypersphere. Note that the requirements for \mathbf{W} in (20) will constrain μ' in a hypercube area, where the following Fig. 13 provides some two-dimensional cases. No matter where μ is located on the hypersphere, the hypercube always has at least half of its volume inside the hypersphere, and in many cases, the volume inside the hypersphere (i.e., gray area) is much larger than that outside it (i.e., pink area).

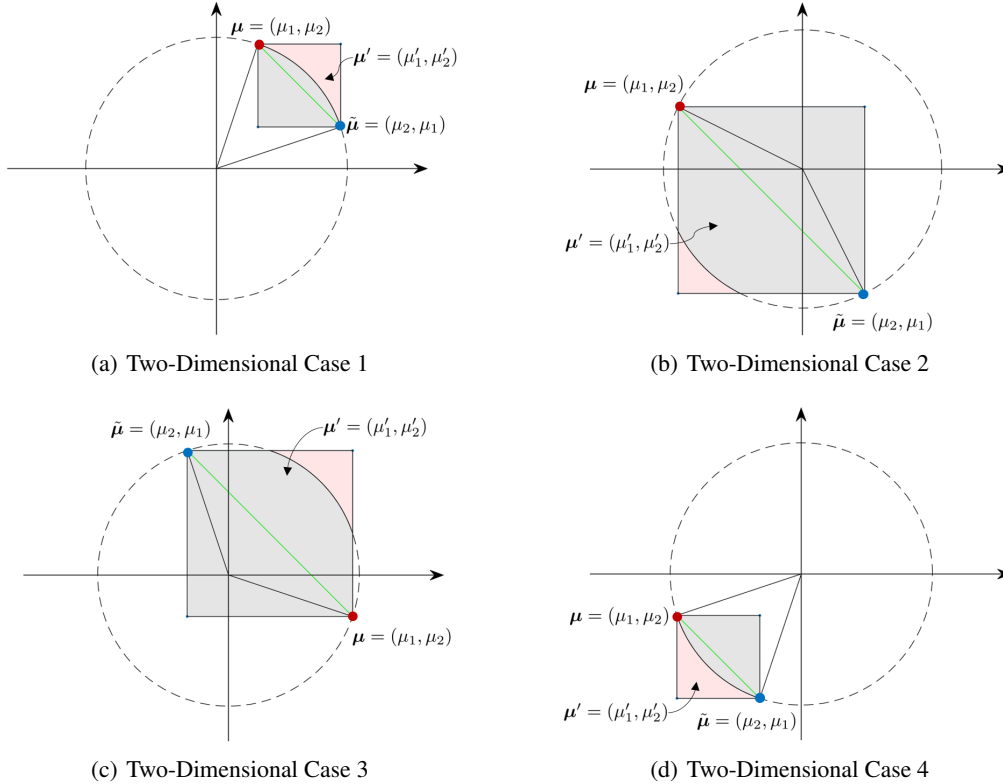


Figure 13. Geometric interpretation for **Proposition 2.1**.

Empirical Verification for Proposition 2.1 The following Fig. 14 demonstrates the distribution of feature means of attacked examples in dataset CIFAR10, under PGD-100 attack ($\epsilon = 8/255$ and step size $\epsilon/10$) through the model trained by MLCAT_{WP} , where the distribution is obtained by kernel density estimation. It can be observed that the distribution center has almost no change, while the variance becomes smaller and smaller with more and more attacking steps, i.e., the shape of the distribution is getting more concentrate.

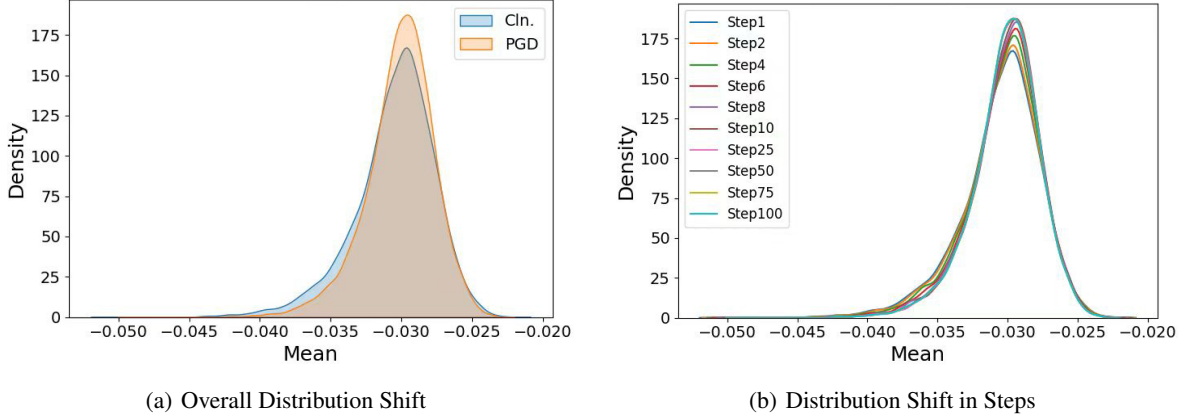


Figure 14. Distribution shift of feature means of attacked examples (average of 512 channels in latent space).

B. Proof of Proposition 2.2

Proposition 2.2 Suppose the set of clean examples $\mathbf{x}_1, \mathbf{x}_2, \dots, \mathbf{x}_N$ are attacked into adversarial examples $\mathbf{x}'_1, \mathbf{x}'_2, \dots, \mathbf{x}'_N$ through a classification model. With a high probability, the mean of feature variances becomes smaller after being attacked.

Proof. For a clean example \mathbf{x}_i and its corresponding adversarial example \mathbf{x}'_i , the feature variances are calculated as

$$\begin{aligned}\sigma_i^2 &= \frac{1}{d} \sum_{j=1}^d (x_{ij} - \mu_i)^2 = \frac{1}{d} \sum_{j=1}^d x_{ij}^2 - \mu_i^2 = \frac{1}{d} (\mathbf{x}_i \mathbf{x}_i^\top) - \mu_i^2, \\ \sigma_i'^2 &= \frac{1}{d} \sum_{j=1}^d (x'_{ij} - \mu'_i)^2 = \frac{1}{d} \sum_{j=1}^d x'^2_{ij} - \mu'^2_i = \frac{1}{d} (\mathbf{x}'_i \mathbf{x}'^\top_i) - \mu'^2_i.\end{aligned}\tag{32}$$

The expectation of σ^2 is estimated as

$$\begin{aligned}\mathbb{E}(\sigma^2) &= \frac{1}{N} \sum_{i=1}^N \left(\frac{1}{d} (\mathbf{x}_i \mathbf{x}_i^\top) - \mu_i^2 \right) \\ &= \frac{1}{Nd} \sum_{i=1}^N (\mathbf{x}_i \mathbf{x}_i^\top) - \frac{1}{N} \mu_i^2 \\ &= \frac{1}{Nd} \text{tr}(\mathbf{X} \mathbf{X}^\top) - \frac{1}{N} \text{tr}(\boldsymbol{\mu} \boldsymbol{\mu}^\top) \\ &= \frac{1}{Nd} \text{tr}(\mathbf{X}^\top \mathbf{X}) - \frac{1}{N} \text{tr}(\boldsymbol{\mu}^\top \boldsymbol{\mu}) \\ &= \Phi_{\sigma^2}.\end{aligned}\tag{33}$$

Similarly, the expectation of σ'^2 is estimated as

$$\mathbb{E}(\sigma'^2) = \frac{1}{Nd} \text{tr}(\mathbf{X}^\top \mathbf{W}^\top \mathbf{W} \mathbf{X}) - \frac{1}{N} \text{tr}(\boldsymbol{\mu}^\top \mathbf{W}^\top \mathbf{W} \boldsymbol{\mu}) = \Phi_{\sigma'^2}.\tag{34}$$

The difference of the two expectations is then computed as

$$\begin{aligned}\mathbb{E}(\sigma^2) - \mathbb{E}(\sigma'^2) &= \frac{1}{Nd} \text{tr}(\mathbf{X}^\top \mathbf{X} - \mathbf{X}^\top \mathbf{W}^\top \mathbf{W} \mathbf{X}) - \frac{1}{N} \text{tr}(\boldsymbol{\mu}^\top \boldsymbol{\mu} - \boldsymbol{\mu}^\top \mathbf{W}^\top \mathbf{W} \boldsymbol{\mu}) \\ &= \frac{1}{Nd} \text{tr}(\mathbf{X}^\top (\mathbf{I} - \mathbf{W}^\top \mathbf{W}) \mathbf{X}) - \frac{1}{N} \text{tr}(\boldsymbol{\mu}^\top (\mathbf{I} - \mathbf{W}^\top \mathbf{W}) \boldsymbol{\mu}).\end{aligned}\tag{35}$$

According to Cauchy-Schwarz Inequality, i.e., $(\sum_{i=1}^n a_i^2)(\sum_{i=1}^n b_i^2) \geq (\sum_{i=1}^n a_i b_i)^2$, there is

$$\frac{1}{d} \sum_{j=1}^d x_{ij}^2 = \frac{1}{d^2} \sum_{j=1}^d x_{ij}^2 \sum_{j=1}^d 1^2 \geq \frac{1}{d^2} \left(\sum_{j=1}^d x_{ij} \right)^2 = \left(\frac{1}{d} \sum_{j=1}^d x_{ij} \right)^2 = \mu_i^2.\tag{36}$$

If **Proposition 2.1** holds, from the proof of **Proposition 2.1**, i.e., Eq. (27), we know that $\boldsymbol{\mu}^\top (\mathbf{I} - \mathbf{W}^\top \mathbf{W}) \boldsymbol{\mu} \geq 0$, thereby

$$\begin{aligned} \mathbb{E}(\sigma^2) - \mathbb{E}(\sigma'^2) &\geq \frac{1}{N} \text{tr}(\boldsymbol{\mu}^\top (\mathbf{I} - \mathbf{W}^\top \mathbf{W}) \boldsymbol{\mu}) - \frac{1}{N} \text{tr}(\boldsymbol{\mu}^\top (\mathbf{I} - \mathbf{W}^\top \mathbf{W}) \boldsymbol{\mu}) \\ &= 0. \end{aligned} \quad (37)$$

□

C. Proof of Proposition 2.3

Proposition 2.3 Suppose the set of clean examples $\mathbf{x}_1, \mathbf{x}_2, \dots, \mathbf{x}_N$ are attacked into adversarial examples $\mathbf{x}'_1, \mathbf{x}'_2, \dots, \mathbf{x}'_N$ through a classification model. With a high probability, the variance of feature variances becomes smaller after being attacked.

Proof. Following the proof of **Proposition 2.1**, we discuss the situation that a series of attacking steps $\mathbf{W}^1, \mathbf{W}^2, \dots, \mathbf{W}^t$ finally lead to the attacking results, i.e., $\mathbf{X}' = \mathbf{W}^t \dots \mathbf{W}^2 \mathbf{W}^1 \mathbf{X} = \mathbf{W}^{(t)} \mathbf{X}$. There is

$$\begin{aligned} \lim_{t \rightarrow \infty} \text{var}(\sigma'^2) &= \lim_{t \rightarrow \infty} \frac{1}{N} \sum_{i=1}^N (\sigma_i'^2 - \Phi_{\sigma'^2}^2) \\ &= \lim_{t \rightarrow \infty} \frac{1}{N} \sum_{i=1}^N \left[\frac{1}{d} (\mathbf{w}_i \mathbf{X} \mathbf{X}^\top \mathbf{w}_i^\top) - (\mathbf{w}_i \boldsymbol{\mu})^2 \right]^2 - \Phi_{\sigma'^2}^2 \\ &= \left[\frac{1}{d} (\beta \mathbf{X} \mathbf{X}^\top \beta^\top) - (\beta \boldsymbol{\mu} \boldsymbol{\mu}^\top \beta^\top) \right]^2 - \Phi_{\sigma'^2}^2 \\ &= 0. \end{aligned} \quad (38)$$

Thus, there is $\lim_{t \rightarrow \infty} [\text{var}(\sigma^2) - \text{var}(\sigma'^2)] \gg 0$. Correspondingly, from the initial state to the extreme state, we can say that $\text{var}(\sigma^2) - \text{var}(\sigma'^2) \geq 0$ with a high probability. □

Empirical Verifications for Propositions 2.2 and 2.3 The following Fig. 15 demonstrates the distribution of feature standard deviations of attacked examples in dataset CIFAR10, under PGD-100 attack ($\epsilon = 8/255$ and step size $\epsilon/10$) through the model trained by MLCAT_{WP}, where the distribution is obtained by kernel density estimation. It can be observed that both the mean and the variance of feature standard deviations become smaller and smaller with more and more attacking steps, i.e., the distribution center is shifting to the left and the shape of the distribution is getting more concentrate.

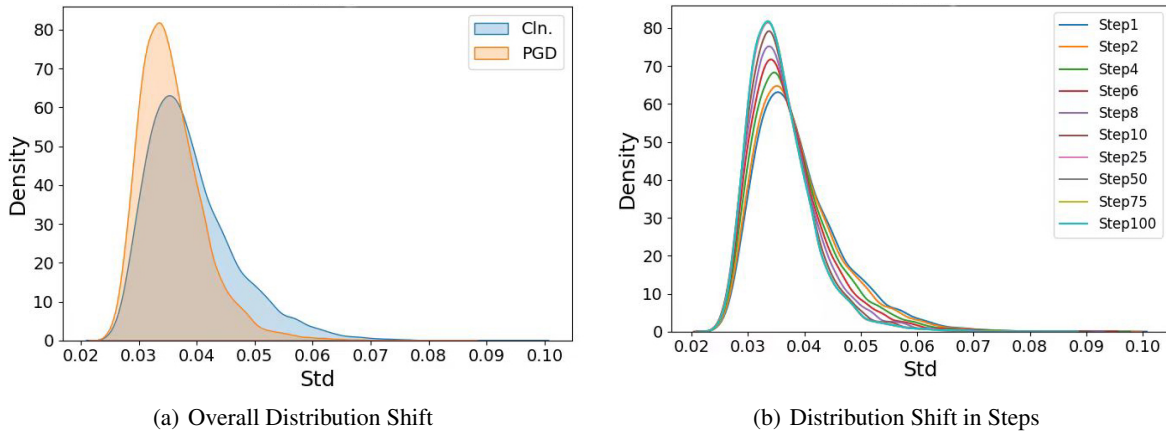


Figure 15. Distribution shift of feature standard deviations of attacked examples (average of 512 channels in latent space).

D. Proof of Theorem 3.1

Theorem 3.1 Let $\hat{\mu}_{b,c}$ and $\hat{\sigma}_{b,c}$ be the reconstructed $\mu_{b,c}$ and $\sigma_{b,c}$ based on Eq. (8), then there are $\text{var}[\hat{\mu}_{b,c}] \geq \text{var}[\mu_{b,c}]$ and $\text{var}[\hat{\sigma}_{b,c}] \geq \text{var}[\sigma_{b,c}]$.

Proof. We derive the distributions of $\hat{\mu}_{b,c}$ and $\hat{\sigma}_{b,c}$. Based on Eq. (7) and Eq. (8) we know that $\hat{\mu}_{b,c}$ and $\hat{\sigma}_{b,c}$ follow independent Gaussian distributions. According to the operation rules for Gaussian distributions, there are

$$\begin{cases} \mathbb{E}[\hat{\mu}_{b,c}] = \mathbb{E}[\mu_{b,c}] + \alpha \cdot \Sigma_{\mu_c} \cdot \mathbb{E}[\epsilon_{\mu}^{b,c}] = \Phi_{\mu_c}, \\ \text{var}[\hat{\mu}_{b,c}] = \text{var}[\mu_{b,c}] + \alpha^2 \cdot \Sigma_{\mu_c}^2 \cdot \text{var}[\epsilon_{\mu}^{b,c}] = (1 + \alpha^2)\Sigma_{\mu_c}^2, \\ \mathbb{E}[\hat{\sigma}_{b,c}] = \mathbb{E}[\sigma_{b,c}] + \beta \cdot \Sigma_{\sigma_c} \cdot \mathbb{E}[\epsilon_{\sigma}^{b,c}] = \Phi_{\sigma_c}, \\ \text{var}[\hat{\sigma}_{b,c}] = \text{var}[\sigma_{b,c}] + \beta^2 \cdot \Sigma_{\sigma_c}^2 \cdot \text{var}[\epsilon_{\sigma}^{b,c}] = (1 + \beta^2)\Sigma_{\sigma_c}^2, \end{cases} \quad (39)$$

from which there are

$$\begin{cases} \hat{\mu}_{b,c} \sim \mathcal{N}(\Phi_{\mu_c}, (1 + \alpha^2)\Sigma_{\mu_c}^2), \\ \hat{\sigma}_{b,c} \sim \mathcal{N}(\Phi_{\sigma_c}, (1 + \beta^2)\Sigma_{\sigma_c}^2). \end{cases} \quad (40)$$

Since $\alpha^2 \geq 0$ and $\beta^2 \geq 0$, there are $\text{var}[\hat{\mu}_{b,c}] \geq \text{var}[\mu_{b,c}]$ and $\text{var}[\hat{\sigma}_{b,c}] \geq \text{var}[\sigma_{b,c}]$, i.e., the variances of both the feature means and standard deviations become larger after reconstruction. \square

E. Datasets

Four publicly available benchmark datasets are used in this paper, i.e., MNIST (LeCun et al., 1998), CIFAR10 (Krizhevsky et al., 2009), SVHN (Goodfellow et al., 2014) and CIFAR100 (Krizhevsky et al., 2009). The details of these datasets are provided in Table 5.

Table 5. Details of the selected datasets.

Dataset	# Training Samples	# Testing Samples	# Classes	# Channels	Image Size
MNIST	60,000	10,000	10	1	28×28
CIFAR10	60,000	10,000	10	3	32×32
CIFAR100	60,000	10,000	100	3	32×32
SVHN	73,257	26,032	10	3	32×32

F. More Experimental Details

F.1. Natural Training for Typical Gradient Attacks

Training and Testing This experiment utilizes a natural training procedure to establish the DNN model, where the classic softmax cross-entropy loss is used. The whole training procedure does not introduce any additional information, including extra data, augmented data, adversarial perturbation, and additional architecture. The only modification is the insertion of the FSU module between two layers of the backbone architecture, which performs a feature reconstruction for each example. The FSU module is also employed for testing (includes attacking and predicting). Since the FSU module only relies on the feature statistics of the current batch, the reconstructions during training and testing do not affect each other.

Reconstruction Positions It is noteworthy that the FSU module can be employed after any hidden layer of the network. Different reconstruction positions may result in different performances. Based on two-fold cross-validation on the training set under FGSM attack:

- For MNIST, we employ the FSU module after the first and second pooling layers during training, and after the first pooling layer during attacking and predicting.
- For CIFAR10, we employ the FSU module after the first convolution block during training, and after the fourth convolution block during attacking and predicting.

- For SVHN, we employ the FSU module after the third convolution block during training, and after the fourth convolution block during attacking and predicting.
- For CIFAR100, we employ the FSU module after the fourth convolution block during training, attacking and predicting.

Random Seeds Since the FSU module involves random sampling from $\mathcal{N}(0, 1)$, the results vary from run to run. In this experiment, the random seed is consistently set as 6666 for all the datasets. We conduct 10 trials and record the mean and standard deviation.

More Visualizations Figs. 16~19 provide more details of the feature maps of randomly selected testing examples attacked by PGD and FGSM. Note that the feature maps are extracted from the layers corresponding to the reconstruction positions. It can be seen that the FSU module does help the attacked examples recover some feature points that possess important semantic information. Especially, from different attacking iterations of PGD in Figs. 16~17, we can see that the adversarial perturbations become stronger and stronger without the FSU module, while with the FSU module, the perturbations have been mitigated to a great extent. Furthermore, from Figs. 18~19, we can see that both the baseline model and the FSU model can provide high-quality feature maps for the clean examples, while under FGSM attack, the feature quality provided by the FSU model is much higher than that of the baseline model.

F.2. Adversarial Training for Powerful Attacks

Training and Testing This experiment does not utilize the FSU module for training. We select several existing state-of-the-art adversarial training methods (i.e., TRADES (Zhang et al., 2019), AT-AWP (Wu et al., 2020), MAIL-TRADES (Wang et al., 2021), and MLCAT_{WP} (Yu et al., 2022)) to establish some robust models, and incorporate the FSU module into the attacking and predicting phases of these models (solution 1), or fine-tune the models by FSU (solution 2). Note that all of these models are trained under the original default parameter settings with the recommended backbone architecture.

Reconstruction Positions It is too time-consuming to cross-validate the reconstruction position for powerful attacks. In this experiment, we consistently apply the feature reconstruction in the latent space for all the datasets, i.e., the FSU module is inserted between the logits layer and the classification layer.

Random Seeds The FSU module in both solution 1 and solution 2 involves random sampling from $\mathcal{N}(0, 1)$. Since it is time-consuming to conduct multiple trials for the powerful attacks, in this section, we conduct single trial for each experiment. With regards to the results of Table 3 (in the main body), the random seed is 0 for TRADES+FSU, AT-AWP+FSU and MLCAT_{WP}+FSU, and is 1 for MAIL-TRADES+FSU. With regards to the results of Table 4 (in the main body), the random seed is 1 for all the fine-tuned models.

G. Codes and Models

All source code required for conducting and analyzing the experiments will be made publicly available at <https://github.com/TechTrekkerZ/FSU> (anonymous link) upon publication of the paper. The well-established models have already been uploaded to this anonymous link.

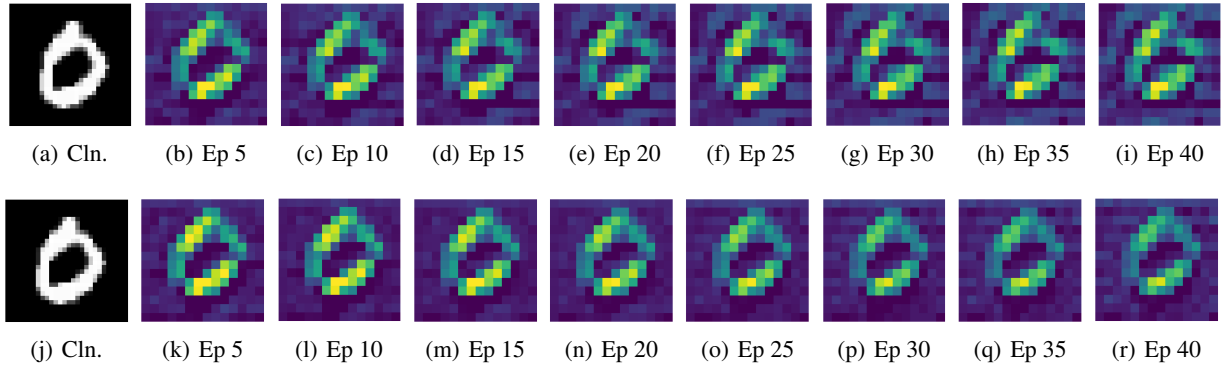


Figure 16. Feature maps of a randomly selected channel for a randomly selected testing example in MNIST during PGD-40 attack (with LeNet-5 backbone). (a)~(i) Baseline-NT. (j)~(r) FSU-NT. (Ep means Epoch.)

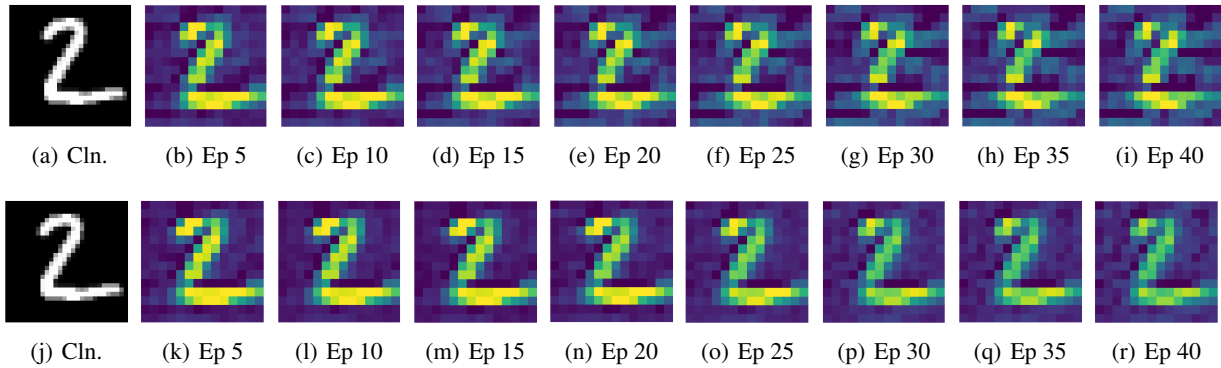


Figure 17. Feature maps of a randomly selected channel for a randomly selected testing example in MNIST during PGD-40 attack (with LeNet-5 backbone). (a)~(i) Baseline-NT. (j)~(r) FSU-NT. (Ep means Epoch.)

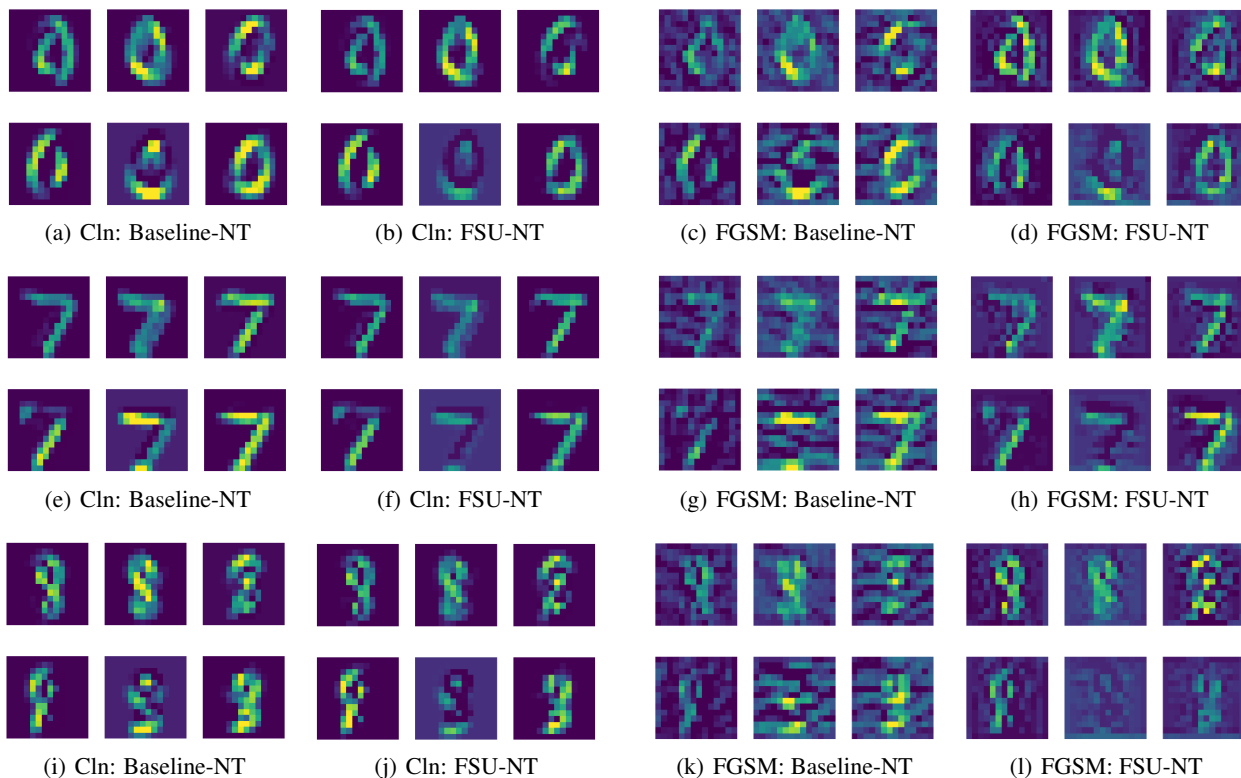


Figure 18. Feature maps of six channels for randomly selected testing examples in MNIST (with LeNet-5 backbone).

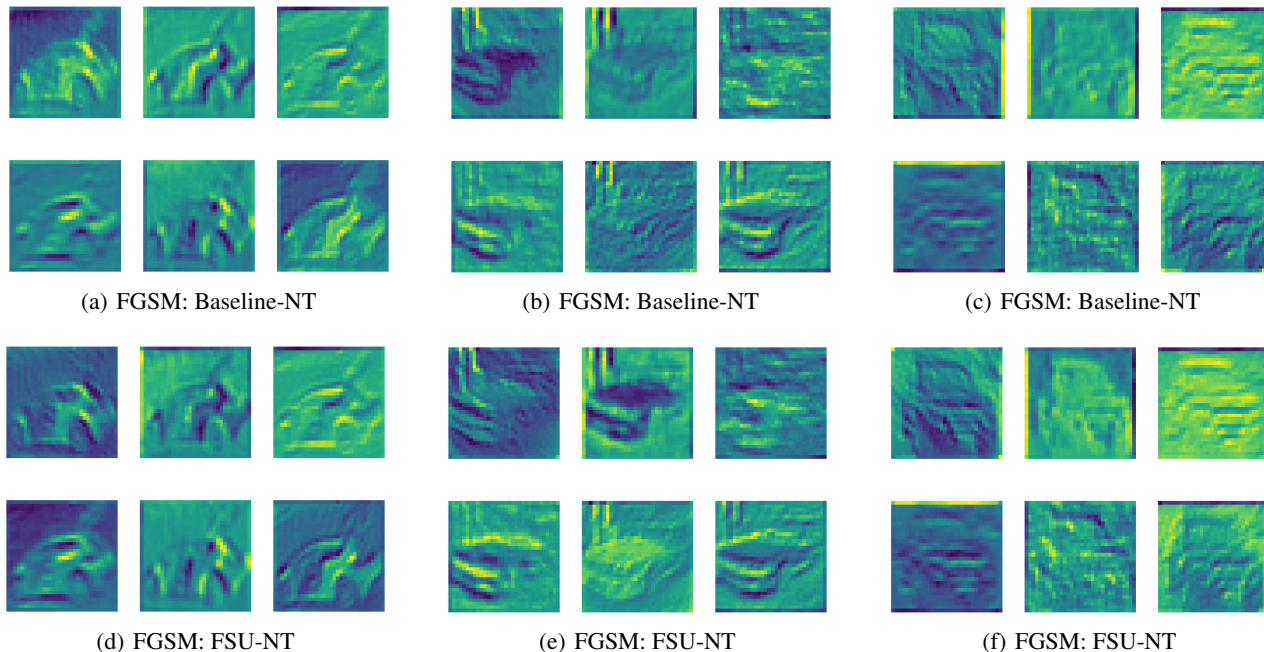


Figure 19. Feature maps of six channels for randomly selected testing examples in CIFAR10 (with ResNet-18 backbone).